Single Particle Tunneling

If the barrier is sufficiently thin (less than 10 or 20Å) there is a significant probability that an electron which impinges on the barrier will pass from one metal to the other: this is called tunneling.

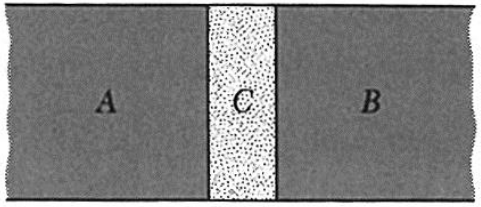

Figure 20 Two metals, *A* and *B*, separated by a thin layer of an insulator *C*.

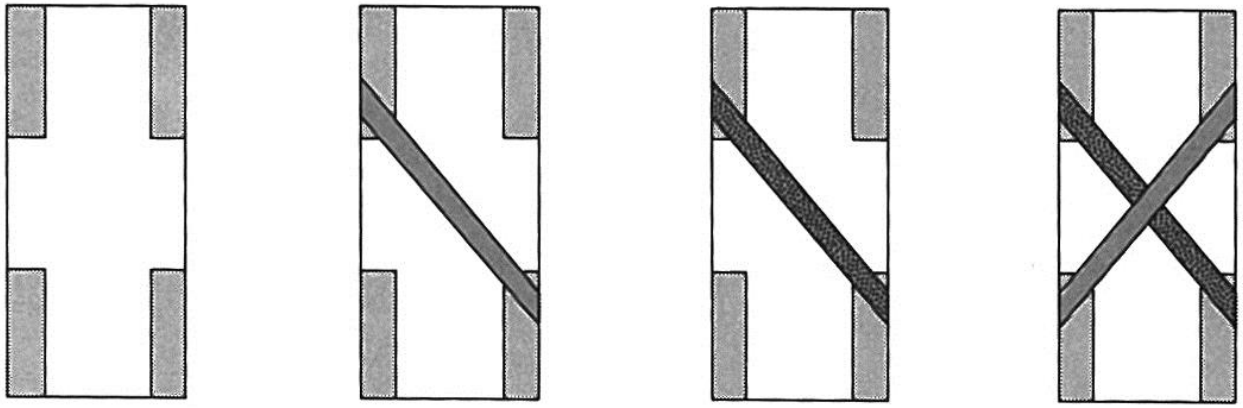

Figure 21 Preparation of an $Al/Al_2O_3/Sn$ sandwich. (a) Glass slide with indium contacts. (b) An aluminum strip 1 mm wide and 1000 to 3000 Å thick has been deposited across the contacts. (c) The aluminum strip has been oxidized to form an Al_2O_3 layer 10 to 20 Å in thickness. (d) A tin film has been deposited across the aluminum film, forming an $Al/Al_2O_3/Sn$ sandwich. The external leads are connected to the indium contacts; two contacts are used for the current measurement and two for the voltage measurement. (After Giaever and Megerle.)

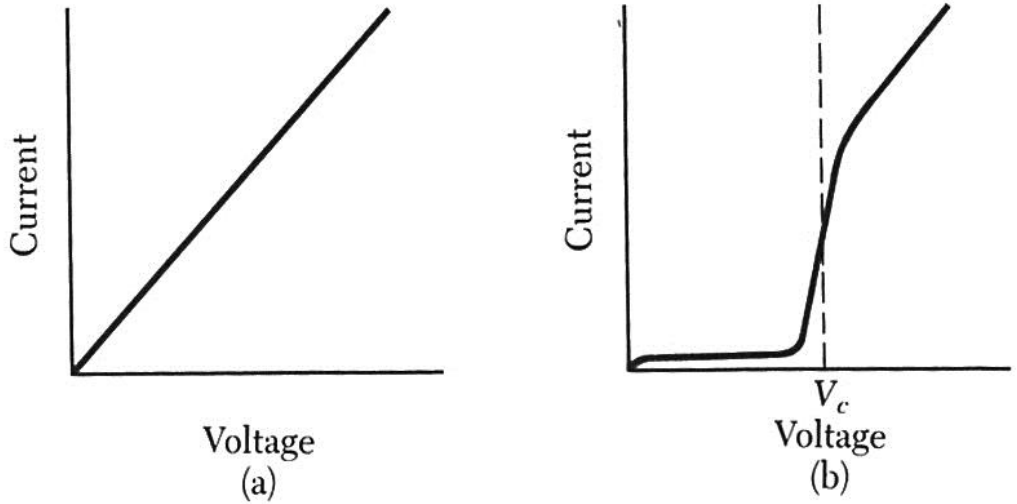

N-N tunneling **S-N tunneling**

Figure 22 (a) Linear current-voltage relation for junction of normal metals separated by oxide layer; (b) current-voltage relation with one metal normal and the other metal superconducting.

1. When both metals are normal conductors, the current-voltage relation of it is Ohmic at low voltages,

2. Giaever (1960) discovered that if one of the metals becomes superconducting, the current-voltage characteristic changes from the straight line of Fig. 22a to the curve shown in Fig. 22b.

Giaever Tunneling

In the superconductor there is an energy gap centered at the Fermi level. At absolute zero no current can flow until the applied voltage is

$$V = Eg/2e = \Delta/e.$$

N (E) = E/ $(E^2-\Delta^2)^{1/2}$

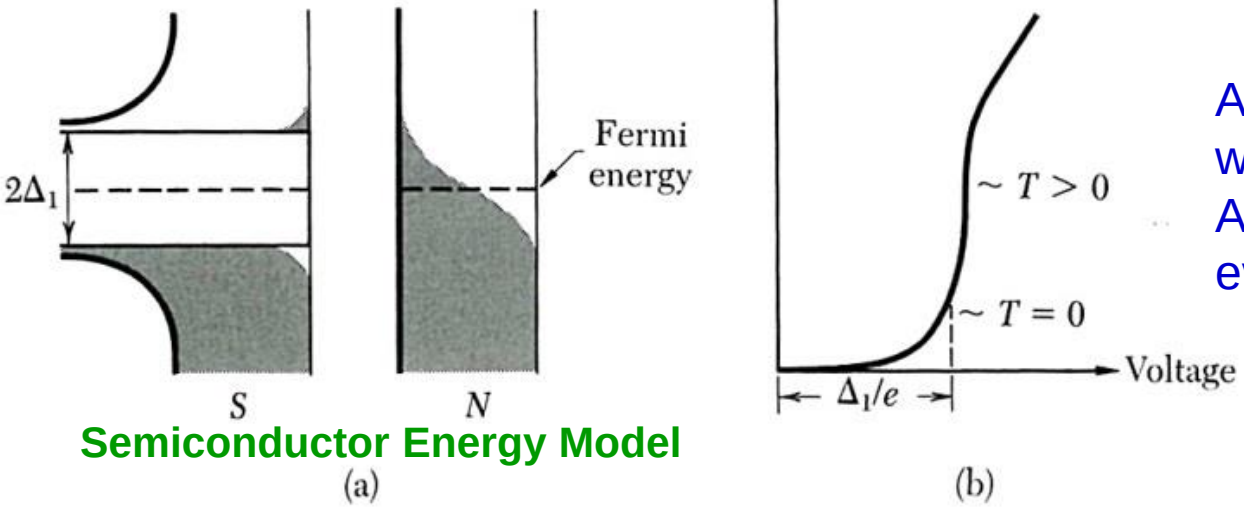

Semiconductor Energy Model

S-N tunneling

At T = 0, **I** is finite when E > Δ,
At T > 0, **I** is > 0 even for E < Δ

Figure 23 The density of orbitals and the current-voltage characteristic for a tunneling junction. In (a) the energy is plotted on the vertical scale and the density of orbitals on the horizontal scale. One metal is in the normal state and one in the superconducting state. (b) I versus V; the dashes indicate the expected break at $T = 0$. (After Giaever and Megerle.)

The current starts when $eV = \Delta$. At finite temperatures, because of electrons in the superconductor that are thermally excited across the energy gap.

Superconducting Tunneling and Application

by L. Solymar

Chapter 4
&
Chapter 5

Semiconductor Model

4.3 Junctions between identical superconductors

The energy diagram for $T = 0°K$ is shown in Fig. 4.4. All energy levels are filled up to $E_F - \Delta$. In thermal equilibrium (Fig. 4.4 (*a*)) there is no current flowing. When a voltage $V < 2\Delta/e$ is applied there is still no current flowing because the electrons below the gap on the left have no access to empty states on the right. At $V = 2\Delta/e$ (Fig. 4.4 (*b*)) there is a sudden rise in current because electrons on the left suddenly gain access to the states above the gap on the right. The corresponding current–voltage characteristic is shown in Fig. 4.4 (*c*).

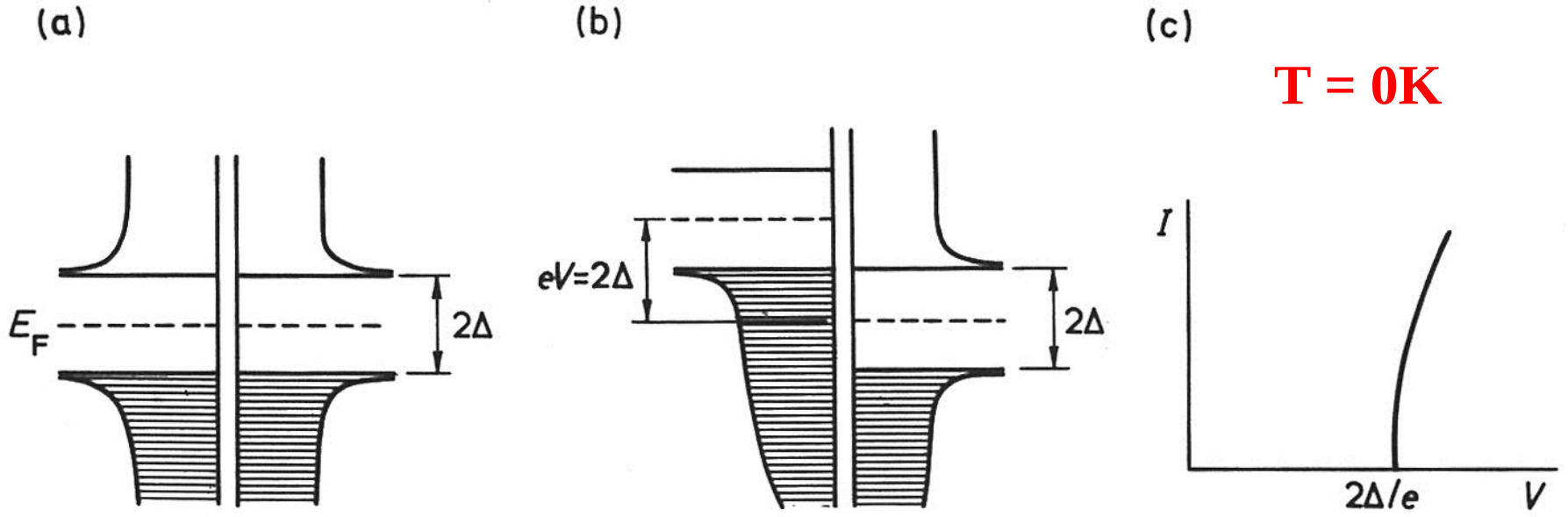

Fig. 4.4 The energy diagram of an SS junction; (*a*) $V = 0$, (*b*) $V = 2\Delta/e$, (*c*) the I–V characteristic at $T = 0$.

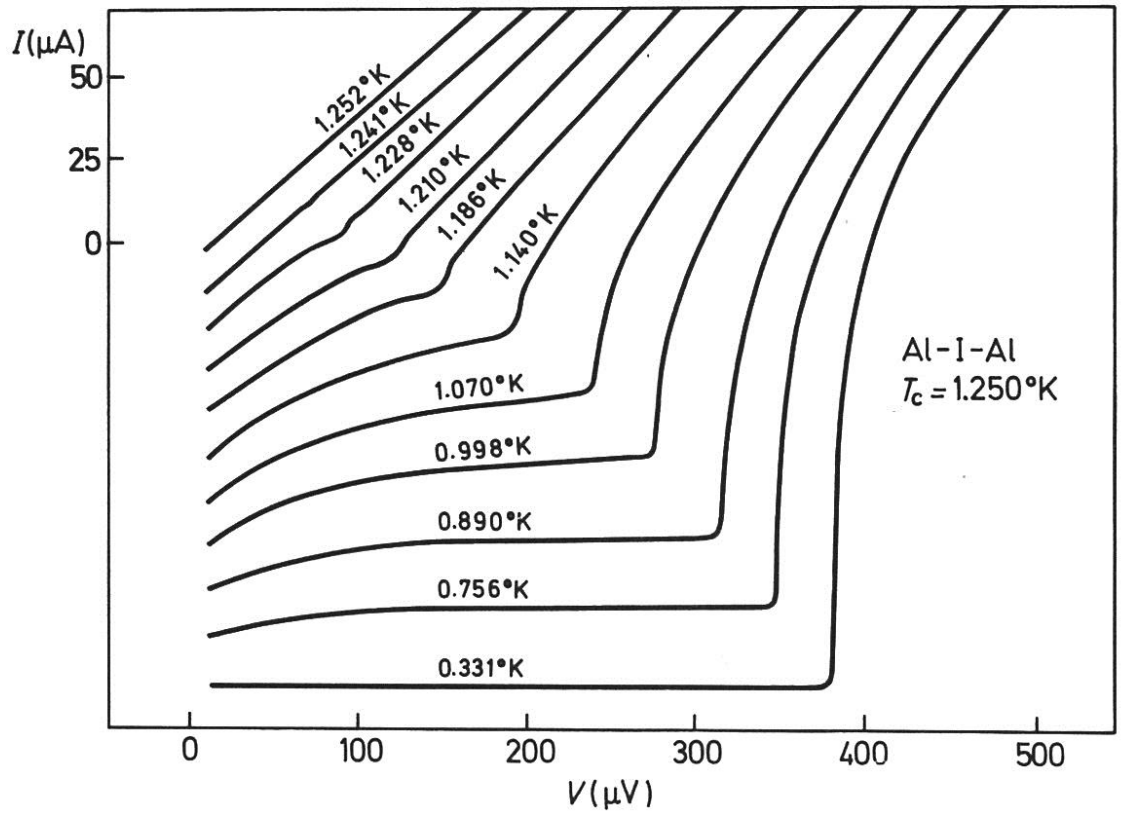

For finite temperatures there will be some rounding off* of the sharp features of Fig. 4.4 (*c*) which, of course, depends on the actual temperature (how near it is to the critical). A very neat set of experimental results (Fig. 4.5) by Blackford and March [99] shows the temperature dependence of the current–voltage characteristic for an aluminium–aluminium oxide–aluminium junction. At 1·252°K aluminium is in the normal state and the characteristic is linear. At 1·241°K (a mere 9 millidegrees below the critical temperature) there is already some sign of the energy gap, and it becomes clearly discernible at 1·228°K. As the temperature decreases the knee in the curves moves to higher and higher voltages (corresponding to higher and higher energy gaps). The characteristic at $T = 0{\cdot}331$°K is practically identical to that at 0°K.

4.4 Junctions between superconductors of different energy gap

In the same way as the previously discussed case of identical superconductors, at $T = 0°K$ no current flows until the applied voltage is sufficiently large to bring the bottom of the gap on the left in line with the top of the gap on the right. This occurs at an applied voltage of $V = (\Delta_1 + \Delta_2)/e$ as shown in Fig. 4.6 (*a*). The current–voltage characteristic (Fig. 4.6 (*b*)) is similar to that shown in Fig. 4.4 (*c*) with the sole difference that the current starts rising at a voltage corresponding to the arithmetical mean of the gap energies.

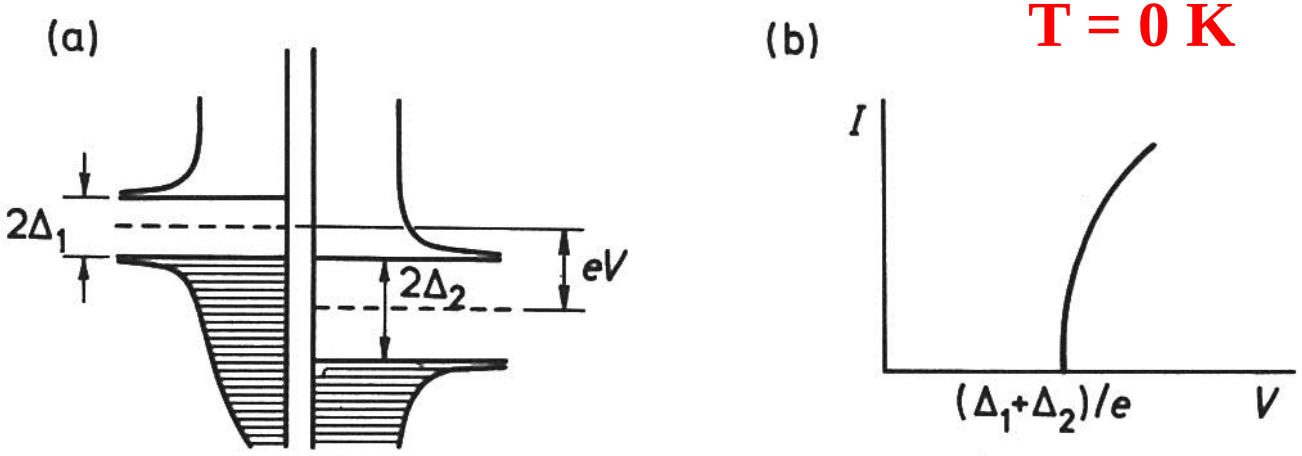

Fig. 4.6 Energy diagram and *I–V* characteristic of an S_1S_2 junction at $T = 0$.

T > 0K

At finite temperatures we may still assume that the normal electron states above the larger gap are empty but there are some thermally excited normal electrons in the smaller-gap superconductor as shown in Fig. 4.7 (*a*) for the case of thermal equilibrium.

Applying a voltage the current will start to flow immediately and will increase with increasing voltage (Fig. 4.7 (*e*)) until $V = (\Delta_2 - \Delta_1)/e$. The energy diagram for this case is shown in Fig. 4.7 (*b*); at this stage all electrons above the gap on the left can tunnel across into empty states on the right. What happens when the voltage is increased further? The number of electrons capable to tunnel across is still the same but they face a smaller density of states, as shown in Fig. 4.7 (*c*), hence the current decreases. The decrease in current continues until $V = (\Delta_1 + \Delta_2)/e$. At this point (Fig. 4.7 (*d*)) electrons from below the gap on the left gain access to empty states on the right, and there is a sudden increase in current. Thus the current–voltage characteristic of Fig. 4.7 (*e*) exhibits a negative resistance in the region

$$\frac{\Delta_2 - \Delta_1}{e} < V < \frac{\Delta_2 + \Delta_1}{e} \tag{3.1}$$

T > 0K

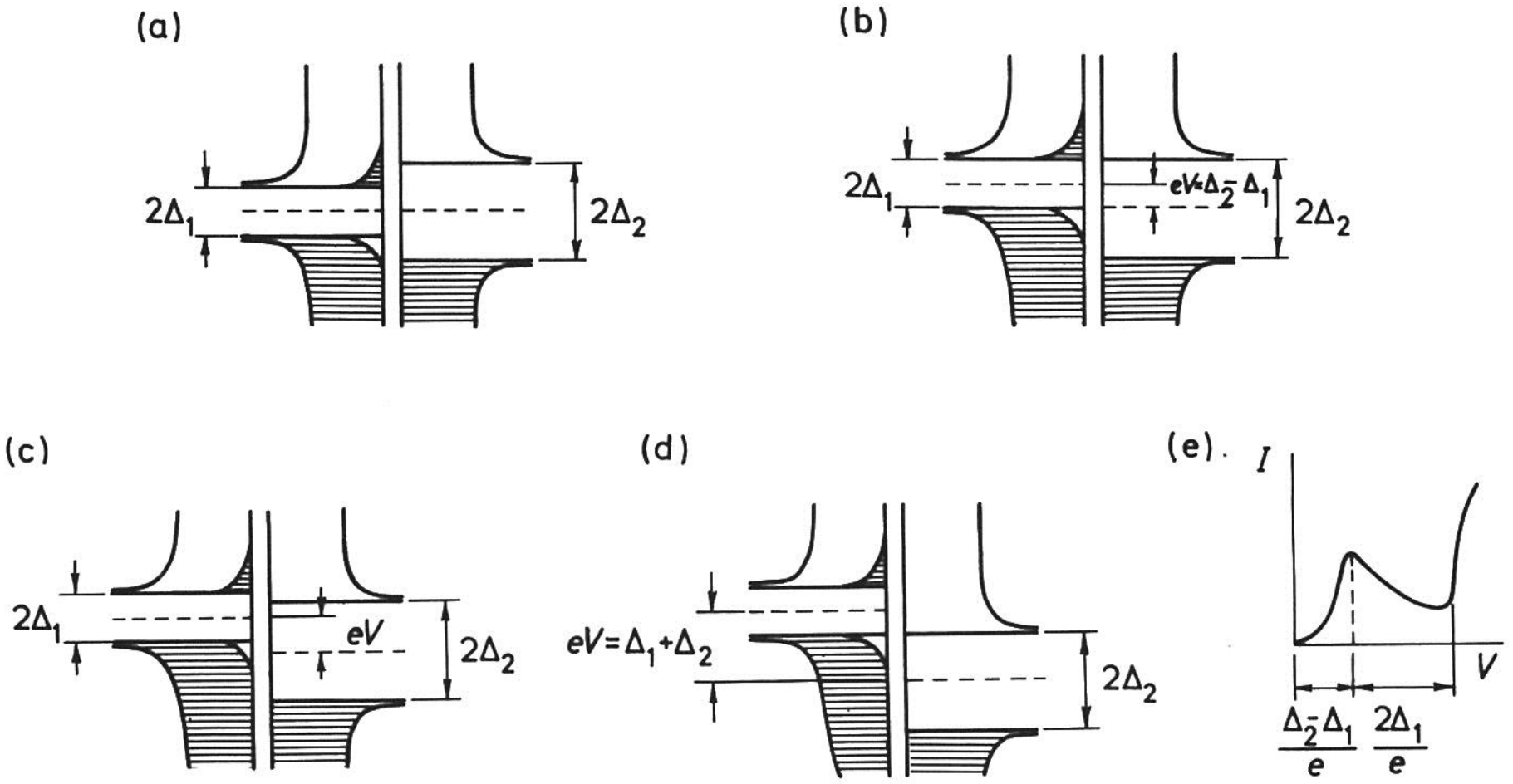

Fig. 4.7 The energy diagram and I–V characteristic of an S_1S_2 junction at finite temperature; (*a*) $V = 0$, (*b*) $V = (\Delta_2 - \Delta_1)/c$, (*c*) $(\Delta_2 - \Delta_1)/e < V < (\Delta_2 + \Delta_1)/e$, (*d*) $V = (\Delta_1 + \Delta_2)/e$, (*e*) the I–V characteristic.

The appearance of a negative resistance was reported simultaneously by Nicol *et al.* [46] and Giaever [45]. A very convincing characteristic presented by the latter author for an Al–Al_2O_3–Pb junction is shown in Fig. 4.8.

The experimentally found dependence [100] of the negative resistance on temperature is shown in Fig. 4.9 for a Sn–SnO–Pb junction. The current–voltage characteristic turns nonlinear when lead becomes superconducting and the negative resistance appears as soon as tin becomes superconducting as well. The negative resistance may be clearly seen down to 2·39°K but not at 1·16°K. Experimentally the negative resistance always disappears at sufficiently low temperatures but that may be due to insufficient accuracy of measurement and to nonideal circumstances.

The presence of a maximum and minimum in the characteristic gives further help in diagnostic measurements aimed at determining the width of the energy gaps. In addition, the negative resistance may be used in devices which will be discussed in more detail in Section 7.1.

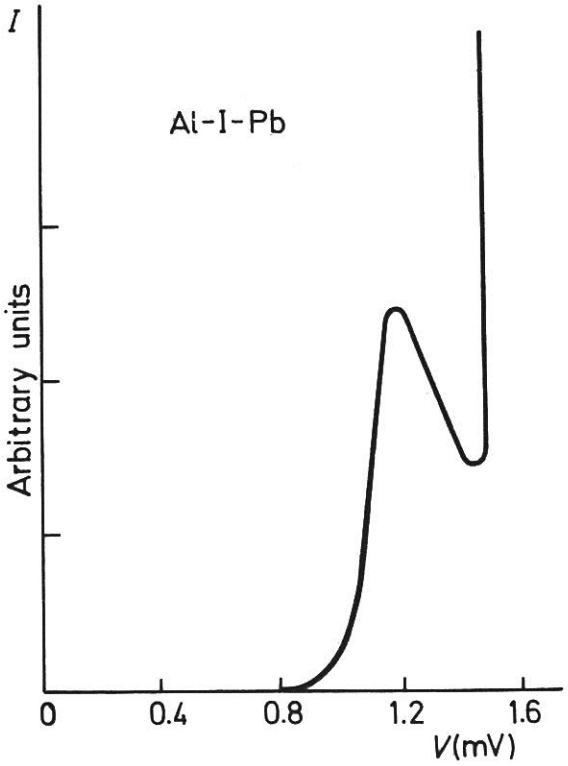

Fig. 4.8 The *I–V* characteristic of an Al–I–Pb junction, both Al and Pb superconducting. After Giaever [45].

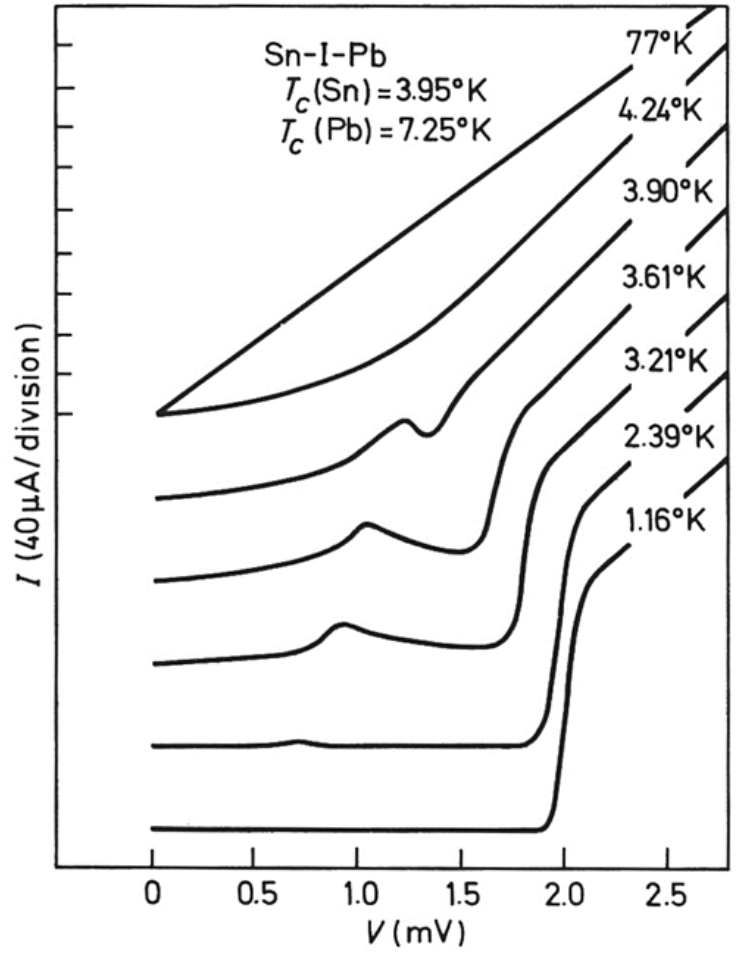

Fig. 4.9 *I–V* characteristics of an Sn–I–Pb junction.

Point contact junctions. These were developed by Levinstein and Kunzler [122, 123] in the form shown in Fig. 4.21. The barrier is prepared by heavily anodising a freshly etched tip of Al, Nb, Ta, etc. The diameter of the junction at the point of contact was estimated to be less than 10 μm. Tunnelling characteristics were observed in a large resistance range from 10^2 to 10^5 ohm.

The advantage of point contacts is that tunnelling measurements can be made on materials not accessible in thin film form. Furthermore, the tunnelling is generally from one single crystal to another since the grain size of the material both in the tip of the point contact and in the bulk is considerably larger than the contact area. Notable success of the point contact technique was to obtain the correct value for the energy gap of Nb_3Sn where thin film measurements consistently gave the wrong value.

was mostly on bulk samples

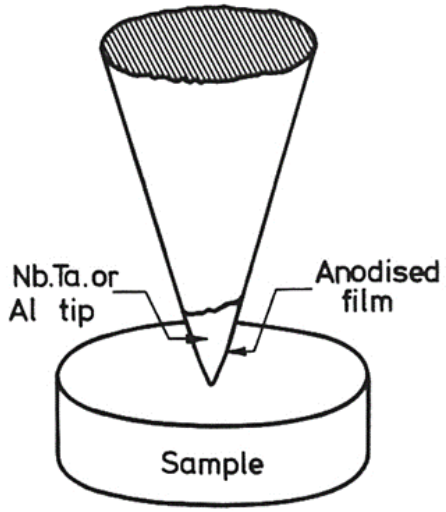

The invention of STM in 1982 !

Fig. 4.21 Point contact junction. After Levinstein and Kunzler [122].

Josephson Superconductor Tunneling

Such a junction is called a weak link.

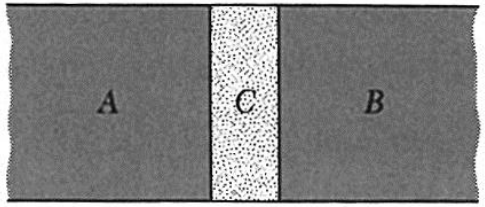

S-I-S
S-N-S

1. **DCJosephson effect**. A dc current flows across the junction in the absence of any electric or magnetic field.
2. **AC Josephson effect**. A dc voltage applied across the junction causes rf current oscillations across the junction.

   An rf voltage applied with the dc voltage can then cause a dc current across the junction.
3. **Macroscopic long-range quantum interference**. A dc magnetic field applied through a superconducting circuit containing two junctions causes the maximum supercurrent to show interference effects as a function of magnetic field intensity. SQUID

DC Josephson Effect. Our discussion of Josephson junction phenomena follows the discussion of flux quantization, let both superconductors be identical.

$$i\hbar \frac{\partial \psi_1}{\partial t} = \hbar T \psi_2 \ ; \qquad i\hbar \frac{\partial \psi_2}{\partial t} = \hbar T \psi_1 \ . \tag{38}$$

Here $\hbar T$ represents the effect of the electron-pair coupling or transfer interaction across the insulator; T has the dimensions of a rate or frequency. It is a measure of the leakage of ψ_1 into the region 2, and of ψ_2 into the region 1.

Let $\psi_1 = n_1^{1/2}\, e^{i\theta_1}$ and $\psi_2 = n_2^{1/2}\, e^{i\theta_2}$. Then

$$\frac{\partial \psi_1}{\partial t} = \tfrac{1}{2} n_1^{-1/2}\, e^{i\theta_1} \frac{\partial n_1}{\partial t} + i\psi_1 \frac{\partial \theta_1}{\partial t} = -iT\psi_2 \ ; \tag{39}$$

$$\frac{\partial \psi_2}{\partial t} = \tfrac{1}{2} n_2^{-1/2}\, e^{i\theta_2} \frac{\partial n_2}{\partial t} + i\psi_2 \frac{\partial \theta_2}{\partial t} = -iT\psi_1 \ . \tag{40}$$

We multiply (39) by $n_1^{1/2}\, e^{-i\theta_1}$ to obtain, with $\delta \equiv \theta_2 - \theta_1$,

$$\frac{1}{2} \frac{\partial n_1}{\partial t} + i n_1 \frac{\partial \theta_1}{\partial t} = -iT(n_1 n_2)^{1/2}\, e^{i\delta} \ . \tag{41}$$

We multiply (40) by $n_2^{1/2}\, e^{-i\theta_2}$ to obtain

$$\frac{1}{2} \frac{\partial n_2}{\partial t} + i n_2 \frac{\partial \theta_2}{\partial t} = -iT(n_1 n_2)^{1/2}\, e^{-i\delta} \ . \tag{42}$$

Now equate the real and imaginary parts of (41) and similarly of (42):

For the real part

$$\frac{\partial n_1}{\partial t} = 2T(n_1 n_2)^{1/2} \sin \delta \; ; \qquad \frac{\partial n_2}{\partial t} = -2T(n_1 n_2)^{1/2} \sin \delta \; ; \tag{43}$$

For the imaginary part

$$\frac{\partial \theta_1}{\partial t} = -T\left(\frac{n_2}{n_1}\right)^{1/2} \cos \delta \; ; \qquad \frac{\partial \theta_2}{\partial t} = -T\left(\frac{n_1}{n_2}\right)^{1/2} \cos \delta \; . \tag{44}$$

If $n_1 \cong n_2$ as for identical superconductors 1 and 2, we have from (44) that

$$\frac{\partial \theta_1}{\partial t} = \frac{\partial \theta_2}{\partial t} \; ; \qquad \boxed{\frac{\partial}{\partial t}(\theta_2 - \theta_1) = 0} \; . \tag{45}$$

The Phase difference is time Independent !

$$\frac{\partial n_2}{\partial t} = -\frac{\partial n_1}{\partial t} \; . \tag{46}$$

the current J of superconductor pairs across the junction depends on the phase difference δ as

$$\boxed{J = J_0 \sin \delta = J_0 \sin (\theta_2 - \theta_1) \; ,} \tag{47}$$

J ∝ dN/dt

where J_0 is proportional to the transfer interaction T. The current J_0 is the maximum zero-voltage current that can be passed by the junction. With no applied voltage a dc current will flow across the junction (Fig. 24), with a value between J_0 and $-J_0$ according to the value of the phase difference $\theta_2 - \theta_1$. This is the **dc Josephson effect**.

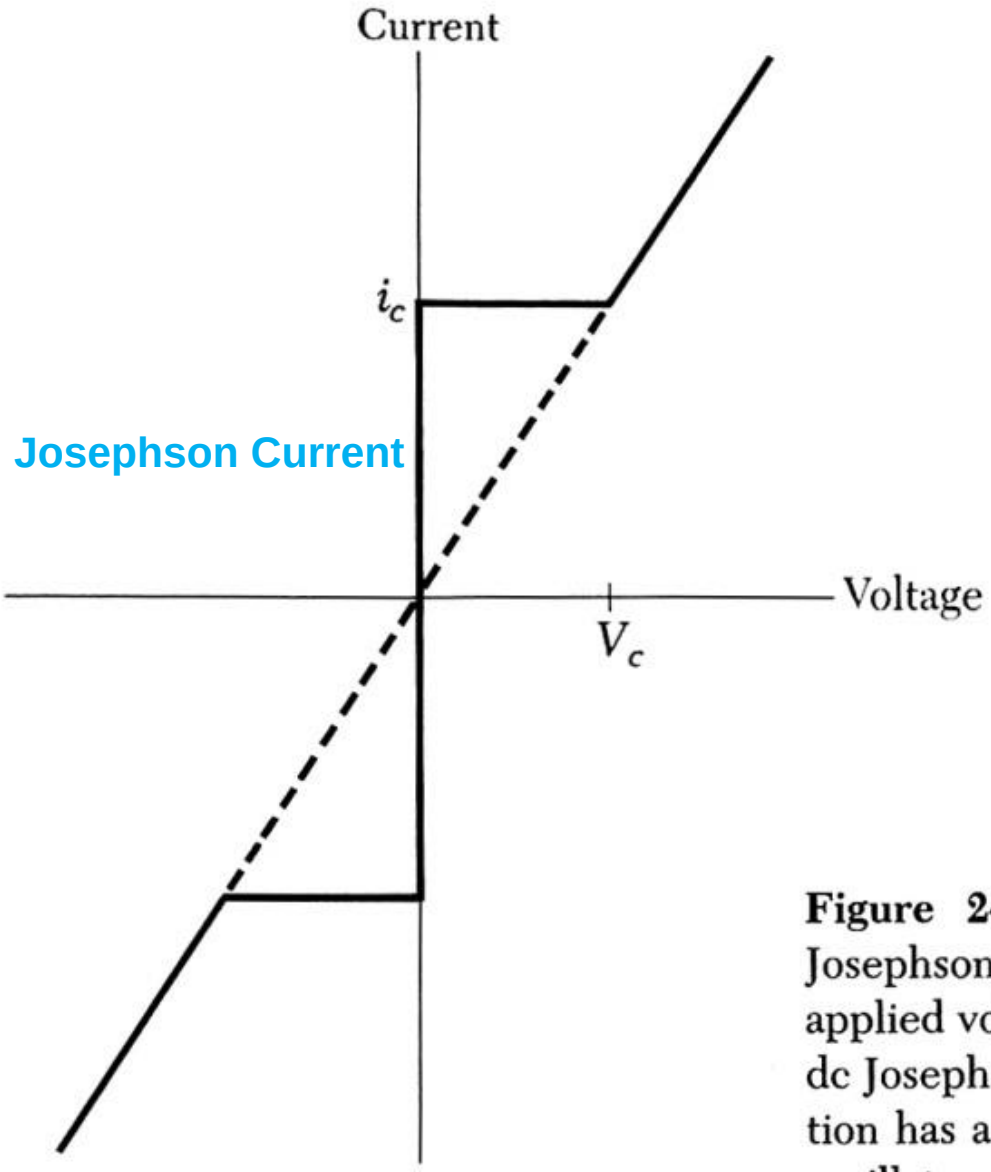

Figure 24 Current-voltage characteristic of a Josephson junction. Dc currents flow under zero applied voltage up to a critical current i_c: this is the dc Josephson effect. At voltages above V_c the junction has a finite resistance, but the current has an oscillatory component of frequency $\omega = 2eV/\hbar$: this is the ac Josephson effect.

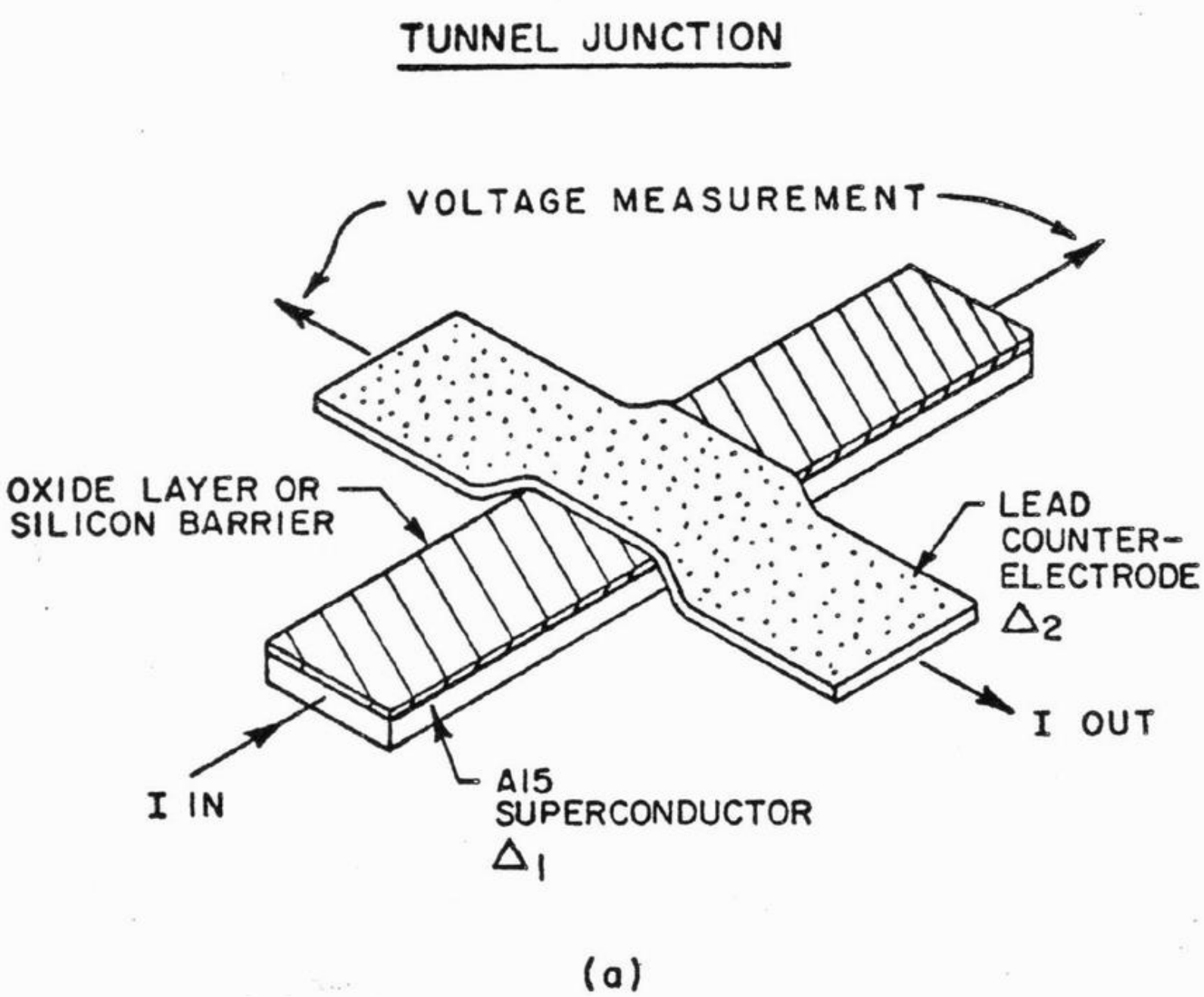

FIG. 1.1--(a) The geometry of our oxide layer tunnel junctions.

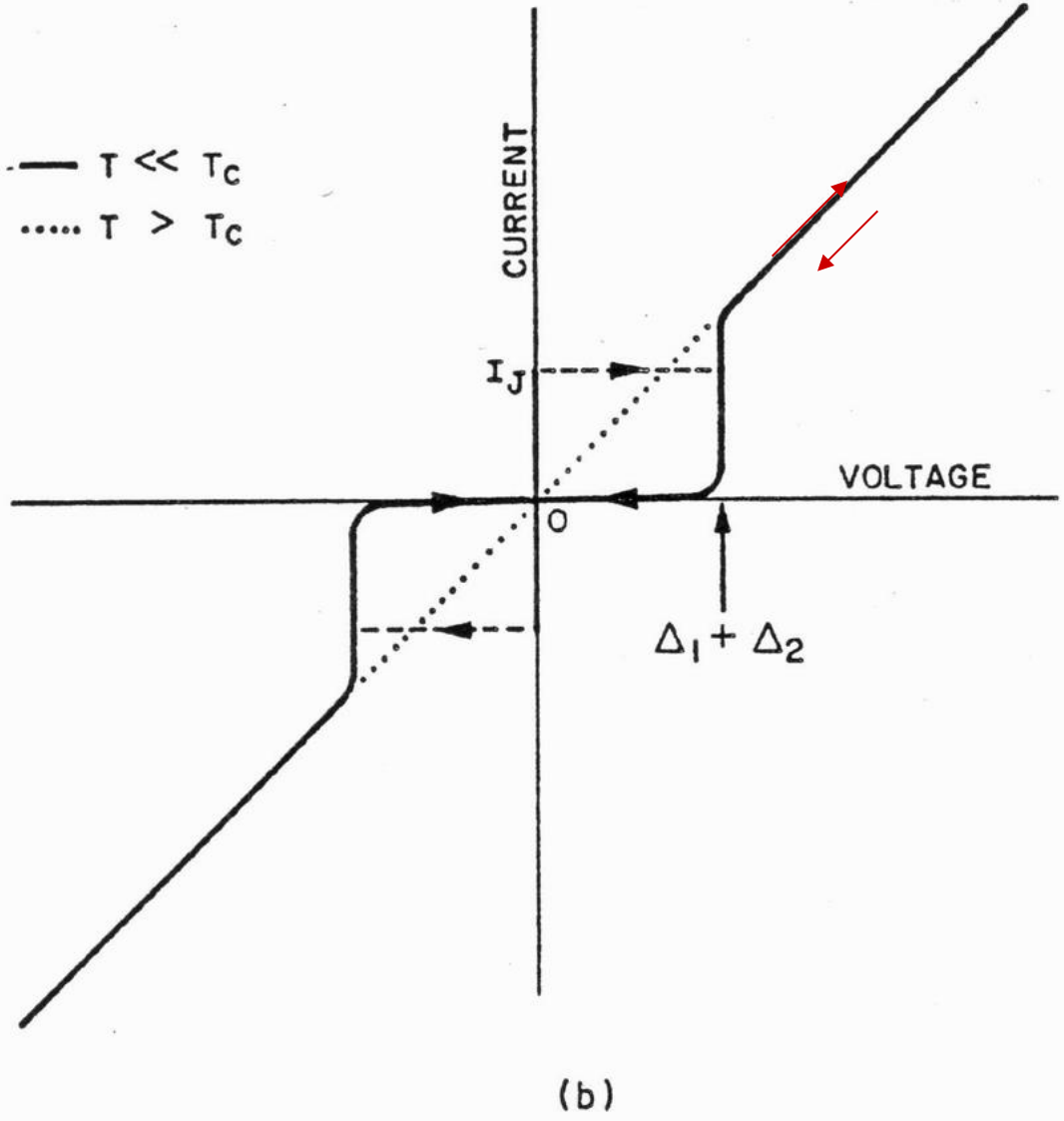

(b)

A Two Terminal Device !

(b) An idealized current-voltage characteristic showing quasiparticle (Giaever) and pair (Josephson) tunneling through the barrier.

AC Josephson Effect.

Under a dc voltage V

We can say that a pair on one side is at potential energy $-eV$ and a pair on the other side is at eV.

$$i\hbar\,\partial\psi_1/\partial t = \hbar T\psi_2 - eV\psi_1; \qquad i\hbar\,\partial\psi_2/\partial t = \hbar T\psi_1 + eV\psi_2 \ . \tag{48}$$

Follow Eq. 41

$$\frac{1}{2}\frac{\partial n_1}{\partial t} + in_1\frac{\partial\theta_1}{\partial t} = ieVn_1\hbar^{-1} - iT(n_1n_2)^{1/2}\,e^{i\delta} \ . \tag{49}$$

This equation breaks up into the real part

$$\partial n_1/\partial t = 2T(n_1n_2)^{1/2}\sin\delta \ , \tag{50}$$

exactly as without the voltage V, and the imaginary part

$$\partial\theta_1/\partial t = (eV/\hbar) - T(n_2/n_1)^{1/2}\cos\delta \ , \tag{51}$$

which differs from (44) by the term $eV/\hbar$.

Follow Eq. 42

$$\frac{1}{2}\frac{\partial n_2}{\partial t} + in_2\frac{\partial\theta_2}{\partial t} = -i\,eVn_2\hbar^{-1} - iT(n_1n_2)^{1/2}\,e^{-i\delta} \ , \tag{52}$$

$$\partial n_2/\partial t = -2T(n_1 n_2)^{1/2} \sin \delta \ ; \tag{53}$$

$$\partial \theta_2/\partial t = -(eV/\hbar) - T(n_1/n_2)^{1/2} \cos \delta \ . \tag{54}$$

with $n_1 \cong n_2$,

$$\partial(\theta_2 - \theta_1)/\partial t = \partial\delta/\partial t = -2eV/\hbar \ . \tag{55}$$

relative phase of the probability amplitudes vary as

$$\delta(t) = \delta(0) - (2eVt/\hbar) \ . \tag{56}$$

$$J = J_0 \sin [\delta(0) - (2eVt/\hbar)] \ . \tag{57}$$

The phase is depending on time.

The current oscillates with frequency

$$\omega = 2eV/\hbar \ . \tag{58}$$

This is the **ac Josephson effect**. A dc voltage of 1 μV produces a frequency of 483.6 MHz. The relation (58) says that a photon of energy $\hbar\omega = 2eV$ is emitted or absorbed when an electron pair crosses the barrier.

To be used for a precise measurement of $\hbar/e$

Macroscopic Quantum Interference.

We consider two Josephson junctions in parallel, as in Fig. 25.

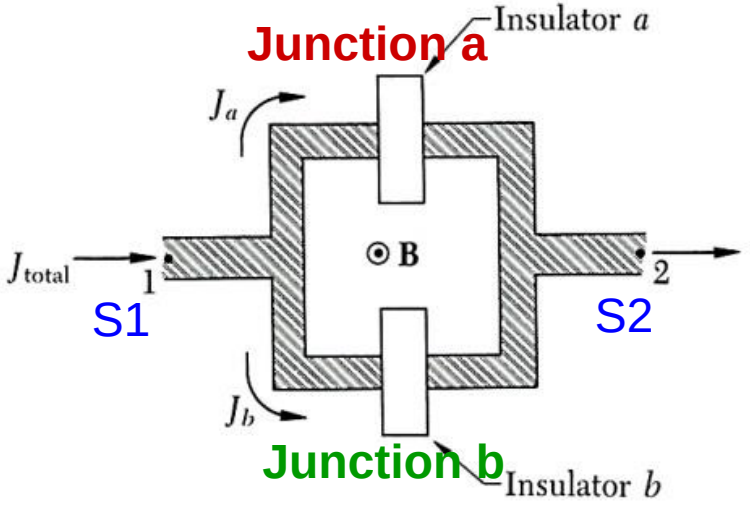

$\theta_1 - \theta_2 = (2e/\hbar c)\Phi$ eq. (59)

Figure 25 The arrangement for experiment on macroscopic quantum interference. A magnetic flux Φ passes through the interior of the loop.

Now let the flux Φ pass through the interior of the circuit.
By (59), $\delta_b - \delta_a = (2e/\hbar c)\Phi$, or

$$\delta_b = \delta_0 + \frac{e}{\hbar c}\Phi \ ; \qquad \delta_a = \delta_0 - \frac{e}{\hbar c}\Phi \ . \tag{60}$$

The total current is the sum of J_a and J_b.

$$J_{\text{Total}} = J_a + J_b = J_0\left\{\sin\left(\delta_0 + \frac{e}{\hbar c}\Phi\right) + \sin\left(\delta_0 - \frac{e}{\hbar c}\Phi\right)\right\} = 2(J_0 \sin \delta_0)\cos\frac{e\Phi}{\hbar c} \ .$$

The current varies with Φ and has maxima when

$$e\Phi/\hbar c = s\pi \ , \qquad s = \text{integer} \ . \tag{61}$$

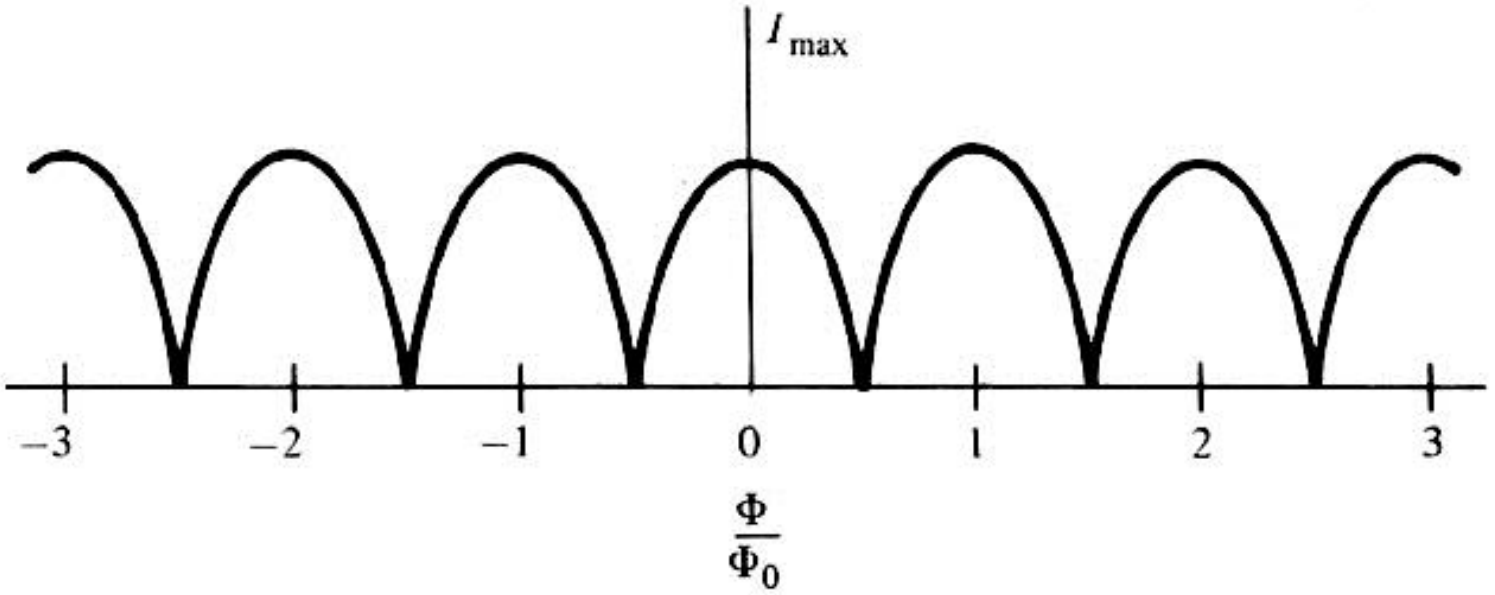

FIGURE 6-5
Dependence of maximum supercurrent through symmetrical two-junction superconducting interferometer (SQUID), shown schematically in Fig. 6-4.

Double slit diffraction pattern for two tunnel junctions

Tinkham, Chapter 6, p. 203

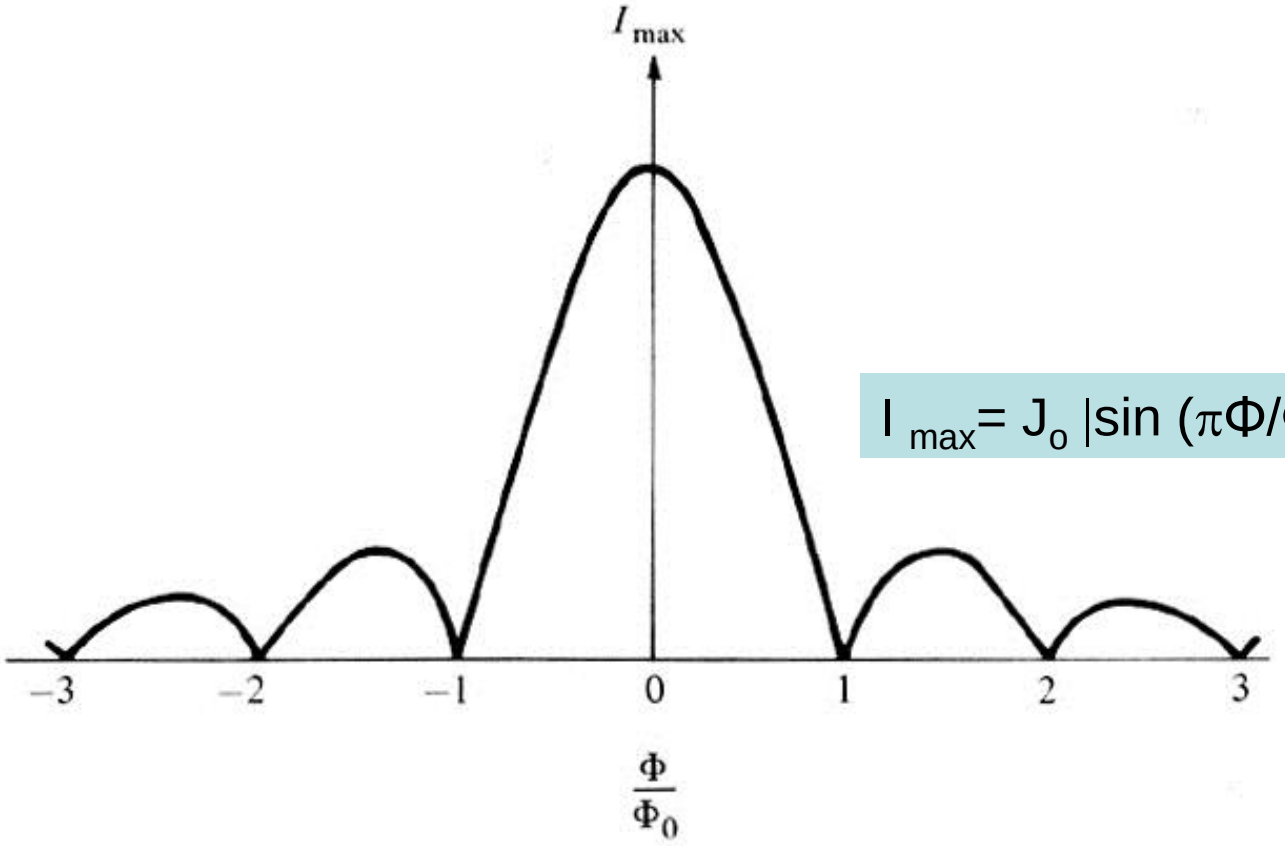

$I_{max} = J_o |\sin(\pi\Phi/\Phi_o)/\pi\Phi/\Phi_o|$

Figure 6-3

Dependence of maximum supercurrent through a single Josephson junction upon the flux threading the junction. The resemblance to the "single-slit" diffraction pattern of optics is evident.

Single slit diffraction for single tunnel junction

Tinkham, Chapter 6, p. 199

The periodicity of the current is shown in Fig. 26.

1. The **short period** variation is produced by interference from the two junctions, as predicted by (61).
2. The **longer period** variation is a diffraction effect and arises from the finite dimensions of each junction.

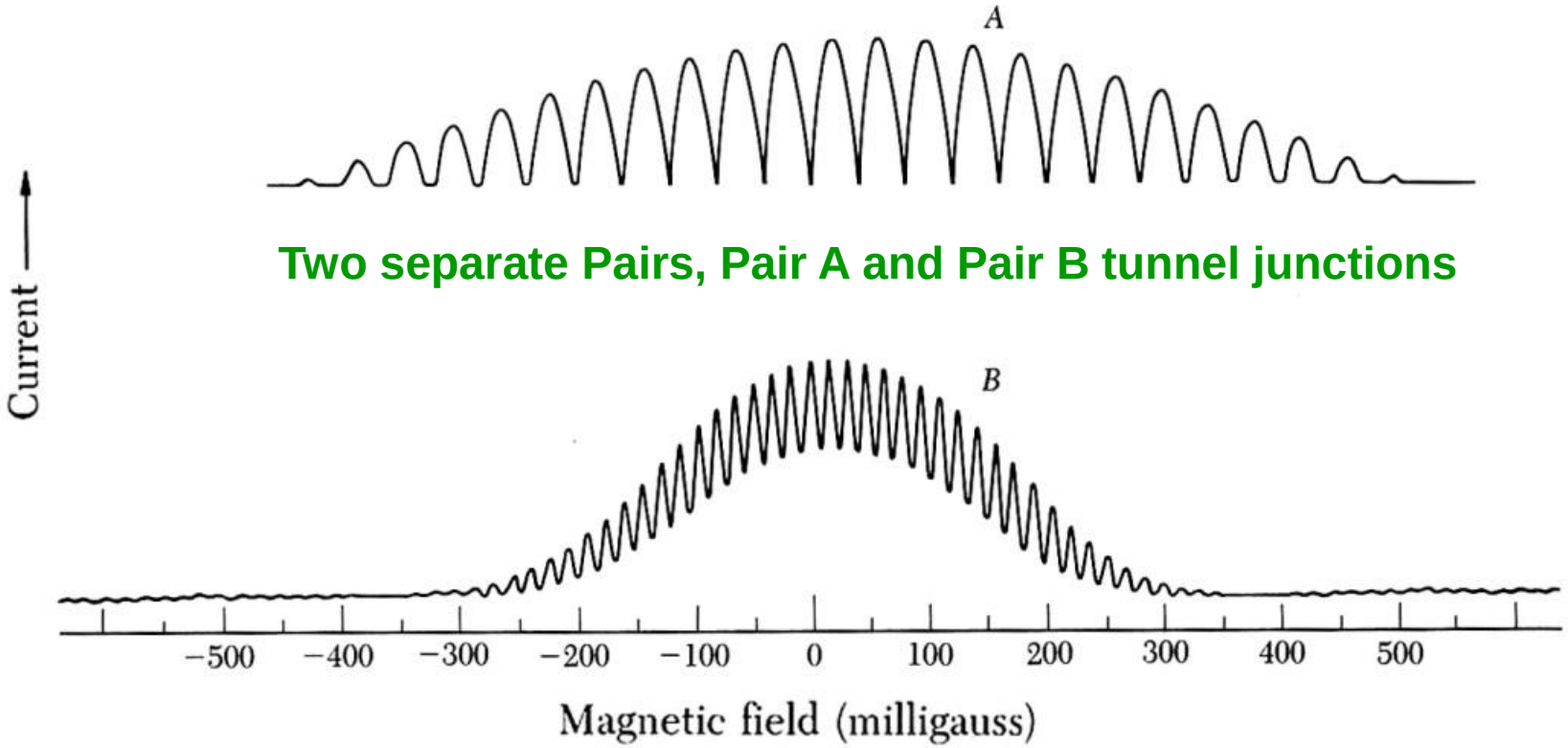

Figure 26 Experimental trace of J_{max} versus magnetic field showing interference and diffraction effects for two junctions A and B. The field periodicity is 39.5 and 16 mG for A and B, respectively. Approximate maximum currents are 1 mA (A) and 0.5 mA (B). The junction separation is 3 mm and junction width 0.5 mm for both cases. The zero offset of A is due to a background magnetic field. (After R. C. Jaklevic, J. Lambe, J. E. Mercereau and A. H. Silver.)

The Discovery of Superconductivity

- Early 90's -- elemental SP metals like Hg, Pb, Al, Sn, Ga, etc.
- Middle 90's -- transitional metals, alloys, and compounds like Nb, NbN, Nb_3Sn, etc.
- Late 90's -- in perovskite oxides

Table 2 Superconductivity of selected compounds

Compound	T_c, in K	Compound	T_c, in K
Nb_3Sn A-15	18.05	V_3Ga	16.5
Nb_3Ge	23.2	V_3Si	17.1
Nb_3Al	17.5	$YBa_2Cu_3O_{6.9}$ HTSC	90.0
NbN B1	16.0	Rb_2CsC_{60}	31.3
K_3C_6O	19.2	La_3In	10.4

Superconductivity tunneling into the A-15 compounds

A-15 compound A_3B, with T_c = 15-23 K

With three perpendicular linear chains of ***A*** atoms on the cubic face, and B atoms are at body centered cubic site

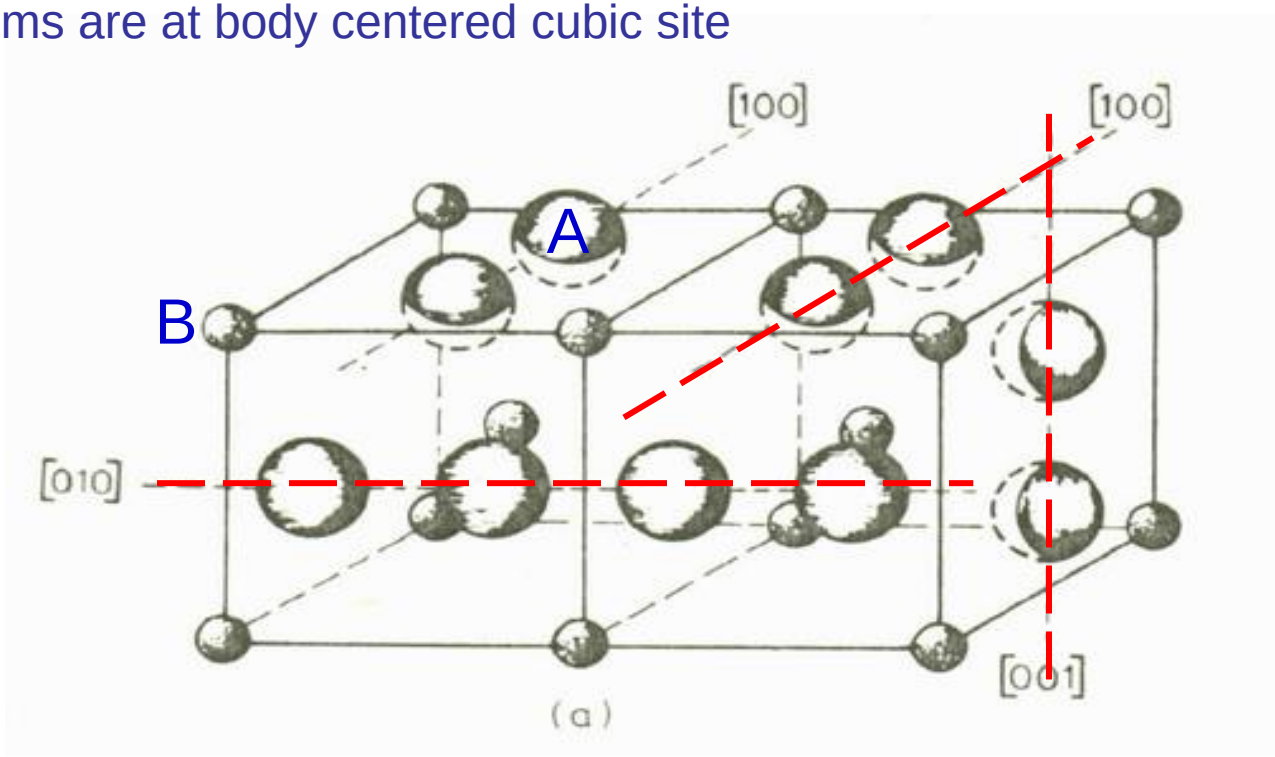

Fig. 34. (a) The position of A and B atoms in the unit cell of an A_3B compound possessing the β-W structure. (b) The Fermi surface of an A_3B compound in the tight binding, nearest neighbors approximation. There are three degenerate bands corresponding to electrons localized on the three families of chains.

1973 Nb_3Ge, 23K !

Low temperature Superconductors

-- Mediated by Electron phonon coupling

-- strong electron phonon coupling, McMillian formula for T_c

$$T_c = \frac{\Theta_D}{1.45} \exp\left\{ - \left[\frac{(1+\lambda_{ep})}{\lambda_{ep} - \mu^*(1+0.62\lambda_{ep})} \right] \right\}$$

λ : electron phonon coupling constant

μ^* : Coulomb repulsion of electrons

$\lambda \propto N(0) < I^2 > / \omega^2$

Are electrons or phonons more important?

Superconductivity tunneling into the A-15 compounds

PHYSICAL REVIEW B VOLUME 23, NUMBER 7 1 APRIL 1981

Superconducting tunneling into the *A*15 Nb_3Al thin films

J. Kwo and T. H. Geballe*
Department of Applied Physics, Stanford University, Stanford, California 94305
(Received 1 October 1980)

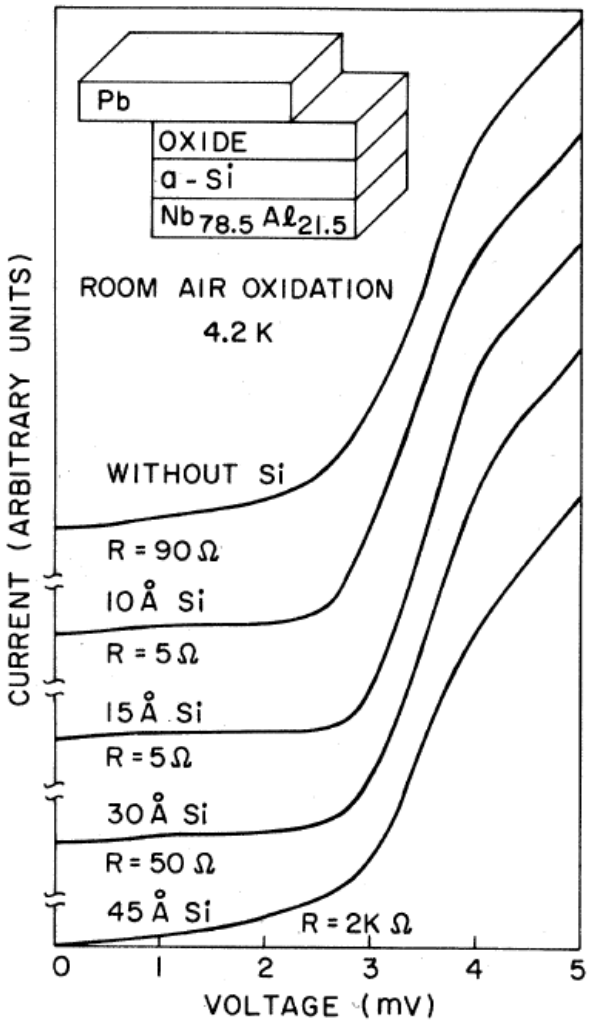

Native Oxide of Nb is no good!

Use of a thin amorphous Si oxide 15A thick, excellent !

Fig. 1 Current-voltage characteristics at 4.2 K of *A*15 Nb-Al (of 21.5 at. % Al) tunnel junctions with the thickness of the *a*-Si overlay varying from 1 to 45 A.

Tunneling as a materials diagnosis

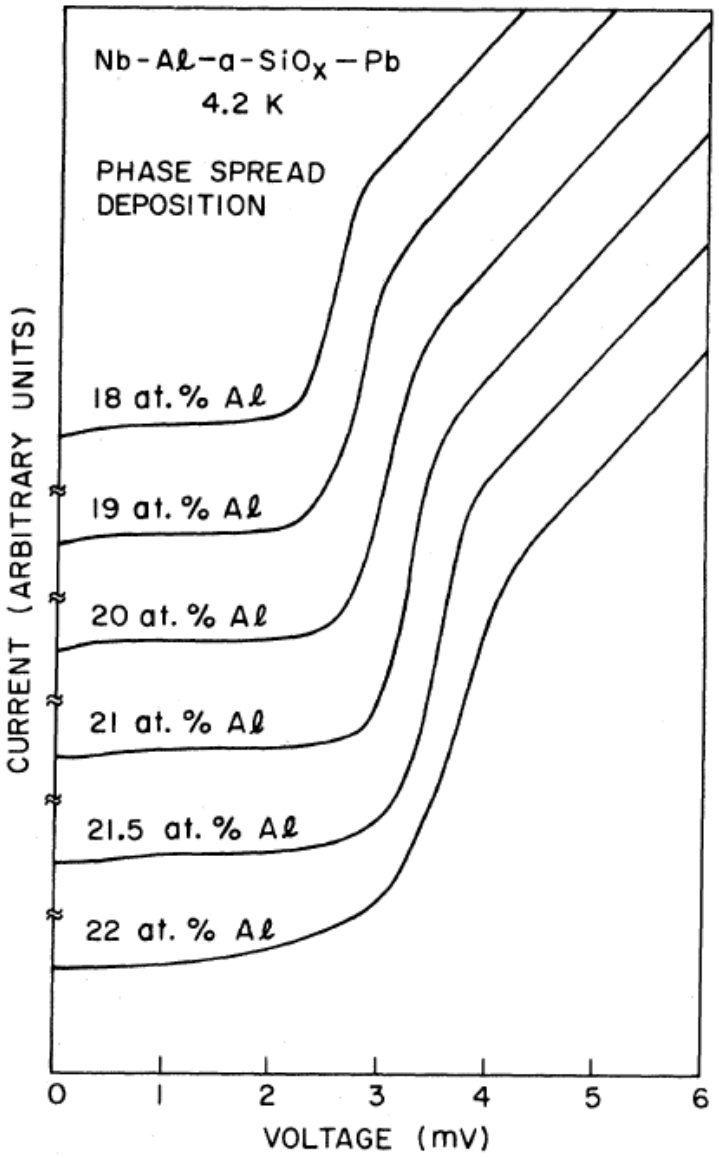

FIG. 2. Current voltage characteristics at 4.2 K of a series of *A*15 Nb-Al junctions obtained from a phase-spread deposition at 950 ℃. The thickness of the *a*-Si overlay is of 15 Å. The *A*15 phase boundary is at 21.8 at. % Al.

Self-Epitaxial Growth

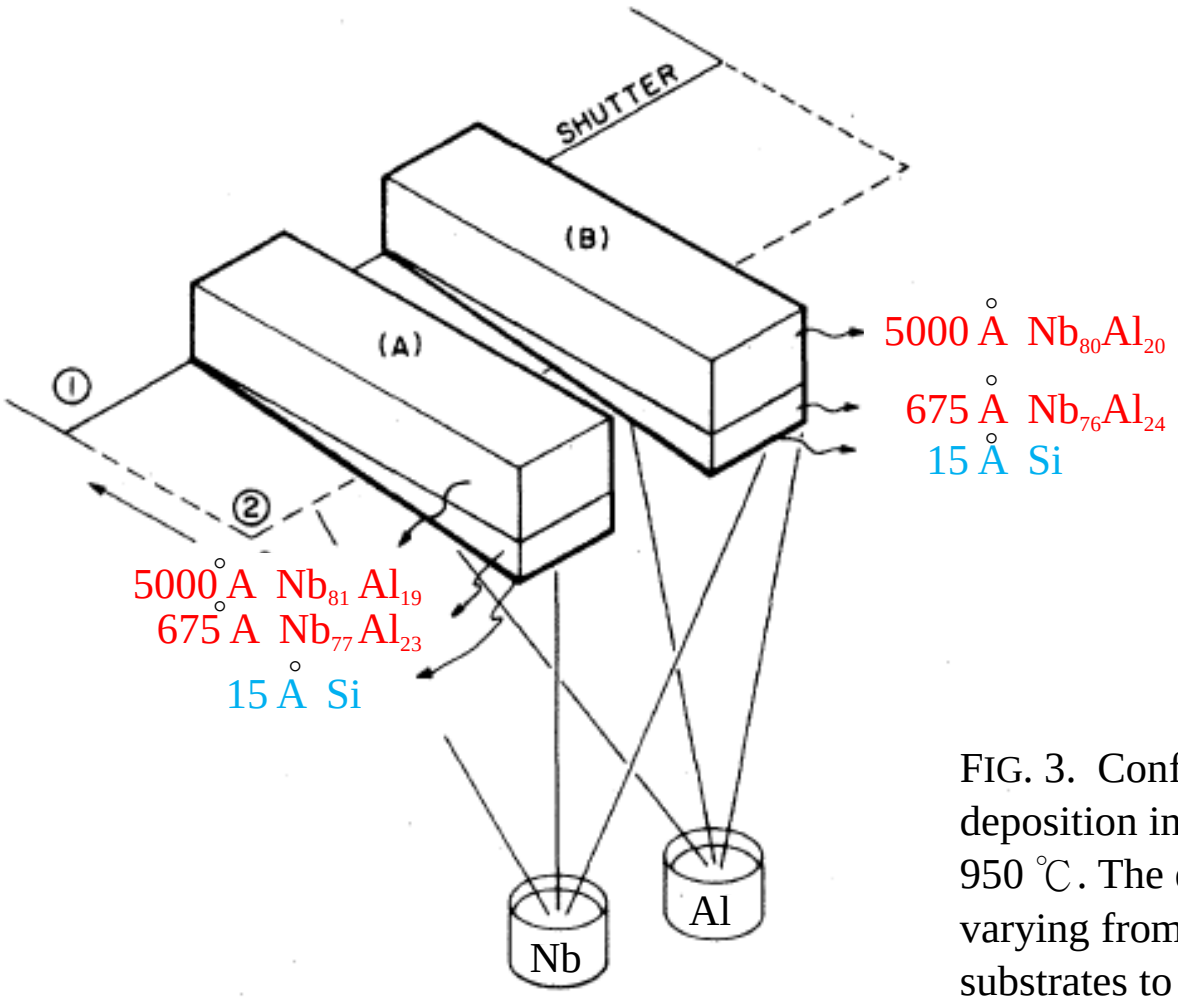

FIG. 3. Configuration for the self-epitaxy deposition in the constant phase direction at 950 ℃. The epitaxial layer thickness is varying from zero at one end of the ten substrates to 675 Å at the other end.

CONSTANT PHASE CONFIGURATION

The use of tunneling to probe the highest T_c layer via self-epitaxial growth

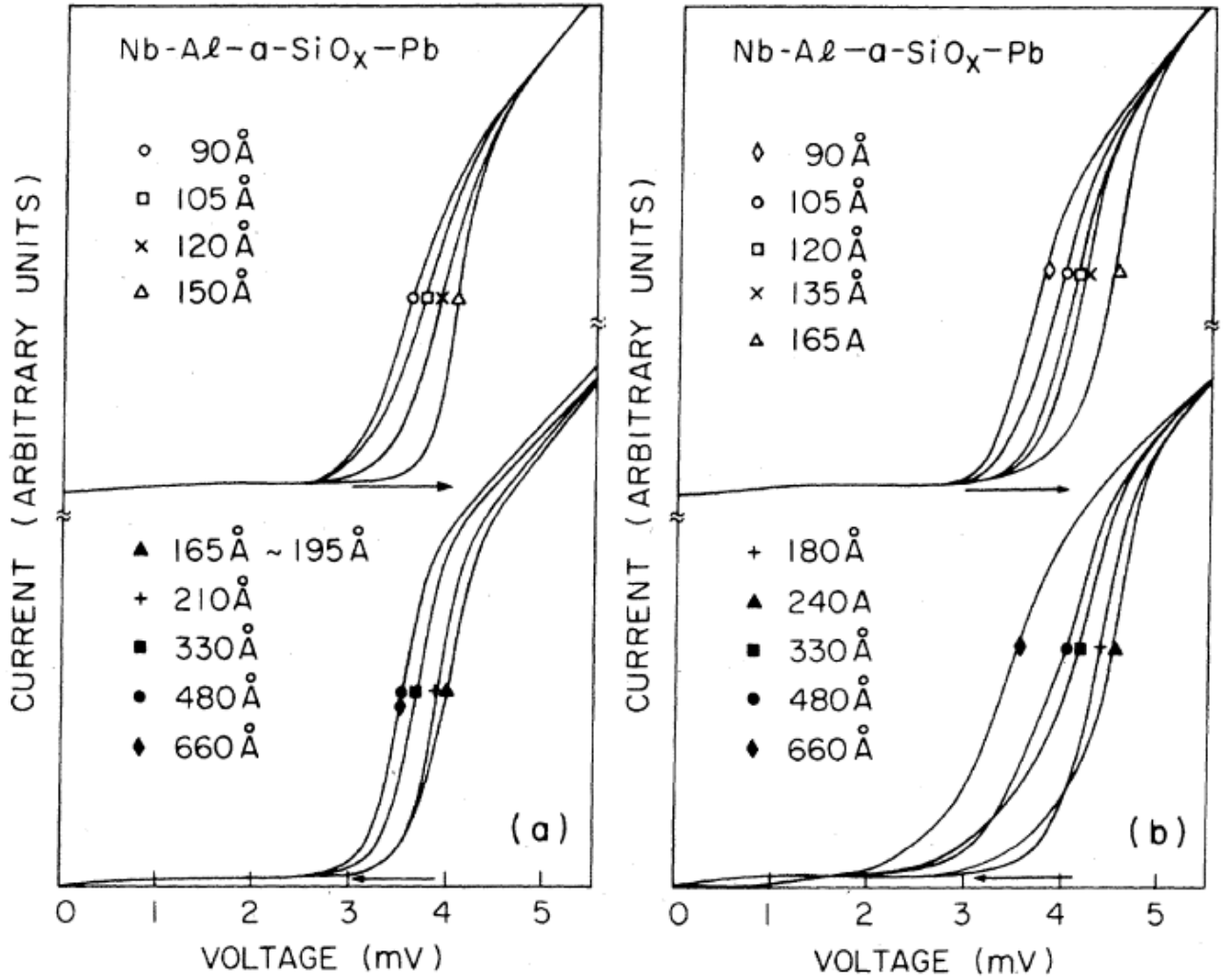

FIG. 4. (a) Current vs voltage at 4.2 K of a series of tunnel junctions on the (*A*)-row self-epitaxial samples with epilayer thickness *d* systematically increasing from 90 to 660 Å. The composition of the epilayer is of 23 at. % Al. (b) The same for the (*B*)-row self-epitaxial sample. The composition of the epilayer is of 24 at. % Al.

Electron –phonon coupling strength vs composition

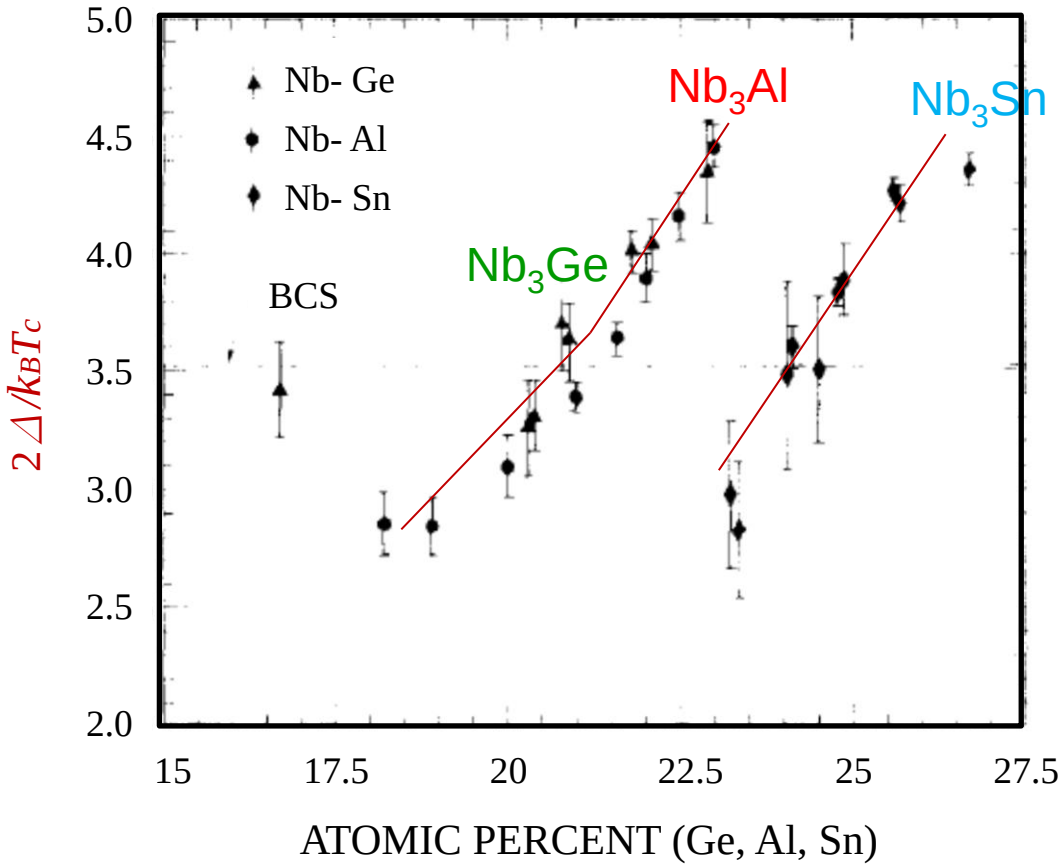

FIG. 2. The variation with composition of the electron-photon coupling strength $2\Delta/k_BT_c$ for the A15 Nb_3Sn, Nb_3Al. And Nb_3Ge. The data are from Rudman et al. [20], Kwo et al. [10], and Khilstrom et al. [11], respectively.

The origin of this dramatic change of the electron phonon coupling strength of Nb_3Al with the composition approaching the *A*15 phase boundary is not well understood. An insight can be gained from referring to the analytical formula by Kresin *et al.*, [21]

$$2\Delta/k_BT_c = 3.53\,[1 + 5.3\,(T_c/\omega_0)^2 \text{ in } (\omega_0/T_c)].$$

which expresses the enhancement of the coupling strength $2\Delta/k_BT_c$ as an explicit function of the ratio T_c/ω_o, where ω_o is a characteristic Einstein phonon frequency. An analysis based on this formula shows that a change in the $2\Delta/k_BT_c$ ratio from BCS-like to a value as large as 4.4 requires a substantial increase in T_c/ω_0. Since T_c varies only modestly, from 14.0 to 16.4 K, the occurrence of phonon-mode softening, i.e., a smaller ω_0 appears to be necessary to account for the large increase in T_c/ω_0. The most direct proof of this supposition is to examine the $\alpha^2F(\omega)$ functions obtained experimentally from tunneling densities of states.

Tunneling density of states and $\alpha^2F(\omega)$

- The dynamic resistance ***dV/dI*** as a function of the bias voltage has been measured for several Nb-Al junctions of importance.
- Data of the superconducting state were taken at 1.5 K with a magnetic field ~ 1 kG applied to quench the superconductivity in Pb.
- Throughout the data reduction, a constant excess conductance, of about 2-5% of the normal-state conductance, was subtracted out from both the superconducting and the normal-state tunneling conductance.
- The reduced tunneling density of states $\boldsymbol{R(\omega)=N_{expt}(\omega)/N_{BCS}(\omega)-1}$ was then calculated.

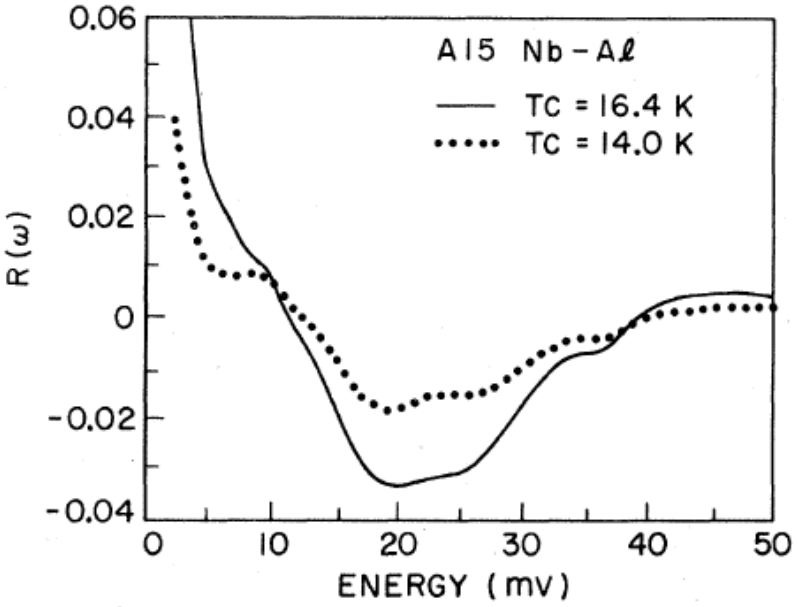

FIG. 6. Reduced tunneling density of states $R(\omega)$ vs energy above the gap for the two Nb-Al junctions of T_c = 16.4 K, Δ =3.15 meV, and T_c = 14.0 K, Δ =2.15 meV, respectively.

- Reduced tunneling density of states $R(\omega)$

  $R(\omega) = N_{exp}(\omega) / N_{BCS}(\omega) - 1$

- *Use $R(\omega)$ and Δ to deduce to $\alpha^2F(\omega)$ by the MR inversion program to extract* λ and μ^*
- *Employ the MMR inversion program to include a normal proximity layer*

- **The electron-phonon spectral function $\alpha^2 F(\omega)$** has been generated from the input data of $R(\omega)$ and Δ by **the gap-inversion analysis** for these two junctions.

- The initial method employed was the conventional McMillan-Rowell inversion program. For the junction with a T_c of 16.4 K and a Δ of 3.15 meV, that analysis gives a value of only 0.6 for the electron-phonon interaction parameter λ, and a negative value ~ -0.10 for the effective Coulomb pseudopotential μ^*. The calculated T_c from these parameters is thus less than 10 K.

- Perhaps the most unphysical result using that analysis is that a high-energy cutoff of less than 30 meV had to be imposed to prevent the iterative solutions from becoming unstable. The structure between 10 and 40 meV, as associated with the Al phonons, was then left out entirely. Furthermore, shown in Fig. 7, there is a large positive offset between the experiment and the calculated $R(\omega)$'s.

Modified McMillan-Rowell (MMR) inversion analysis :

- Based on the model of **proximity-effect tunneling**, proposed by Arnold and implemented by Wolf, it has permitted an improved description, i.e., more self-consistent, of the tunneling data of such Nb and Nb_3Sn junctions within the conventional framework of the strong-coupling theory.
- In this model a thin layer of weakened superconductivity is proposed to exist between the insulating oxide and the base electrode, and it is characterized by a constant pair potential $\Delta_n << \Delta_s$ and a thickness of $d_n << \xi$.
- It is plausible that a thin proximity layer exists between the Nb_3Al film and the *a*-Si oxide barrier. With no a priori knowledge about this proximity layer, we approximate it with $\Delta_n = 0$.
- The tunneling density of states is then, dependent on two additional parameters of

$2d_n/\hbar V_F$ and d_n/l , where d_n , V_F and l are the thickness, the renormalized Fermi velocity, and the mean free path of the proximity layer, respectively.

The reduced tunneling density of states $R(\omega)=N_{expt}(\omega)/N_{BCS}(\omega)-1$ was then calculated. Figure 6 shows the $R(\omega)$'s for two particular junctions. One is a relatively weak coupled superconductor, with a T_c of 14.0 K and a gap of 2.15 meV; the other is strong coupled, of larger Al composition by 1.3 at. %, with a higher T_c at 16.4 K and a gap of 3.15 meV. A reduction in the magnitude of $R(\omega)$ is found as the Al composition is decreased, indicating a weakening in the electron-phonon coupling strength. However, the overall shapes of the two $R(\omega)$'s are rather similar, and there is no dramatic change in the positions of structures induced by phonons. Similar behavior is found in the tunneling densities of states of Nb_3Sn junctions of different T_c's and coupling strength.

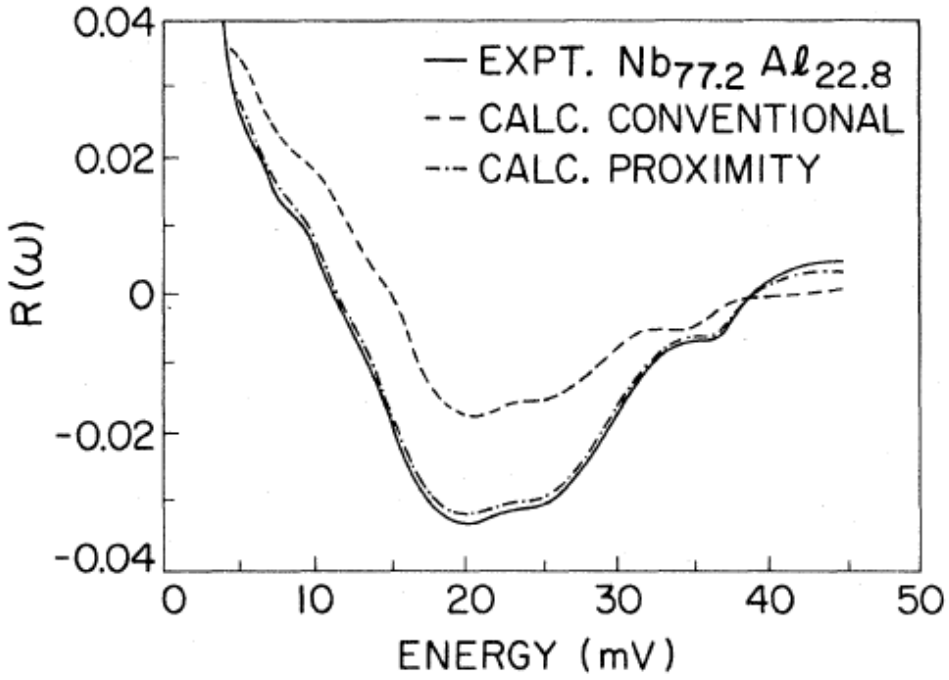

FIG. 7. The experimental and calculated tunneling densities of states $R(\omega)$'s from both conventional and proximity inversion analysis for the $A15$ Nb-Al junction of 22.8 at. % Al with T_c = 16.4 K, Δ =3.15 meV.

Features of the $\alpha^2 F(\omega)$ functions of these two junctions are quite similar, with a slight reduction of about 10% in the $\alpha^2 F(w)$ for the lower-T_c one.

However the strong-coupled and high-T_c junction shows a pronounced enhancement in the weightings of the low-frequency phonons, leading to smaller values of the frequency moments. In fact, the significant reduction of λ, from 1.7 to 1.2 in the lower-T_c junction, is mainly from the stiffening of phonons; i.e., $< \omega^2 >$ of larger by 20%.

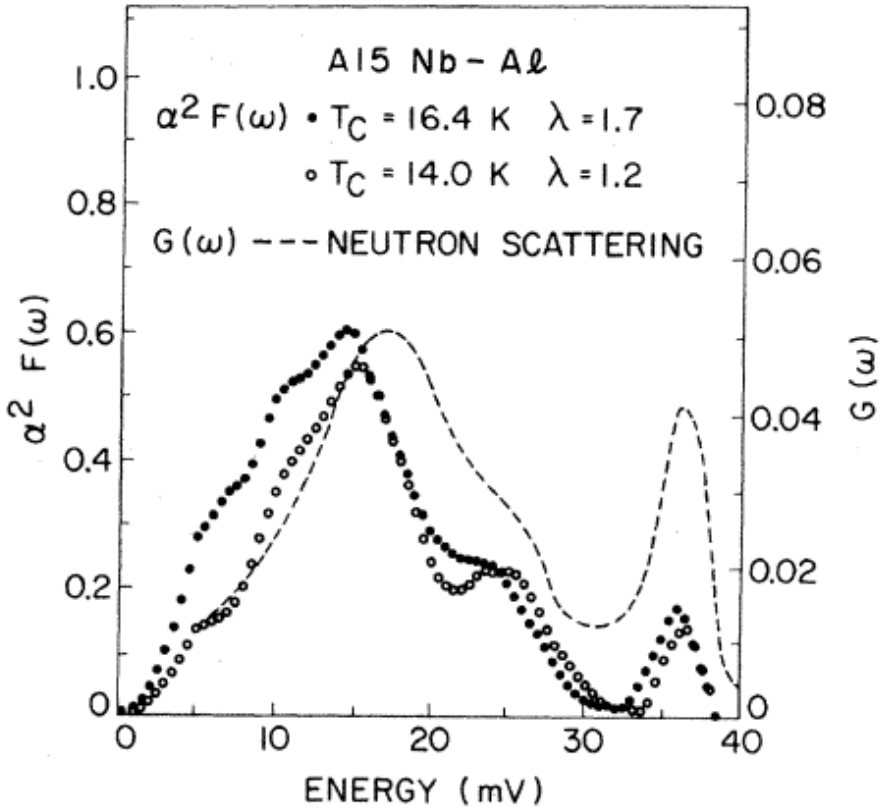

FIG. 8. The electron phonon spectral functions $\alpha^2 F(\omega)$ for two Nb-Al junctions with $2\Delta/k_B T_c$ of 3.6 and 4.4. The data of the neutron scattering function $G(\omega)$ are after Schweiss *et al.*

TABLE I. A summary of the parameters from the proximity inversion analysis of two *A*15 Nb-Al junctions and one Nb_3Sn junction.

	Composition	T_c (K) (expt)	Δ (meV) (expt)	$\frac{2\Delta}{k_B T_c}$ (expt)	λ	μ^*	$\omega_{\log}^{b}$ (meV)	$\langle\omega\rangle^{b}$ (meV)	$\langle\omega^2\rangle^{b}$ $(\text{meV})^2$	T_c (K)[c] (calc)	$\frac{2\Delta}{k_B T_c}$ (calc)	$\frac{2d_n}{\hbar v_F^*}$ $(\text{meV})^{-1}$	$\frac{d_n}{l}$
*A*15 Nb-Al	21.5 at.% Al	14.0 ± 0.2	2.15	3.56	1.2 ± 0.05	0.13 ± 0.01	11.2	13.3	226	11.7	3.8	0.0055	0.065
	22.8 at.% Al	16.4 ± 0.1	3.15	4.45	1.7 ± 0.05	0.15 ± 0.02	9.5	11.4	181	15.1	4.3	0.006	0.055
*A*15 Nb-Sn	25.0 at.% Sn	17.7 ± 0.1	3.25	4.26	1.8 ± 0.15	0.16 ± 0.03	10.8	13.1	226	16.7	4.25	0.0097	0.13

$$T_c = \frac{\Theta_D}{1.45} \exp\left\{-\left[\frac{(1+\lambda_{ep})}{\lambda_{ep} - \mu^*(1+0.62\lambda_{ep})}\right]\right\}$$

the analytical formula by Kresin *et al.*,

$$2\Delta/k_B T_c = 3.53\,[1 + 5.3\,(T_c/\omega_o)^2 \text{ in } (\omega_o/T_c)]$$

which expresses the enhancement of the coupling strength $2\Delta/k_B T_c$ as an explicit function of the ratio T_c/ω_o, where ω_o is a characteristic Einstein phonon frequency.

$$^{a}\lambda = 2\int d\omega\omega^{-1}\alpha^2 F(\omega).$$

$$^{b}\omega_{\log} = \exp\left[\frac{2}{\lambda}\int d\omega\omega^{-1}\ln\omega\alpha^2 F(\omega)\right] .$$

$$^{c}T_c = \frac{\langle\omega\rangle}{1.2}\exp\left[\frac{-1.04(1+\lambda)}{\lambda - \mu^*(1+0.62\lambda)}\right] , \text{ see Ref. 30.}$$

$$\lambda = N(0) \langle I^2 \rangle / M\langle\omega^2\rangle$$

- The electron-phonon coupling constant λ can be expressed according to McMillan, as $\lambda = N^b(0)\langle I^2\rangle / M(\omega^2)$

, where $N^b(0)$ and $\langle I^2\rangle$ are the electronic band density of states, and the electron-phonon matrix element, evaluated over the Fermi surface, respectively.

- The electronic parameter $N^b(0)$ (bare) can be estimated from the renormalized density of states $N^*(0)$ by specific heat experiments

$$C_{el} = 1/3\ \pi^2 N^*(0) K_B^2\ T$$

$$N^b(0)\left[\frac{\text{states}}{\text{eV spin unit cell}}\right] = \frac{17.8}{1+\lambda}\gamma^{*M}\left[\frac{\text{mJ}}{\text{cm}^3\text{K}^2}\right],$$

Also from upper critical field analysis, given that the (1+ λ) factor is known from tunneling.

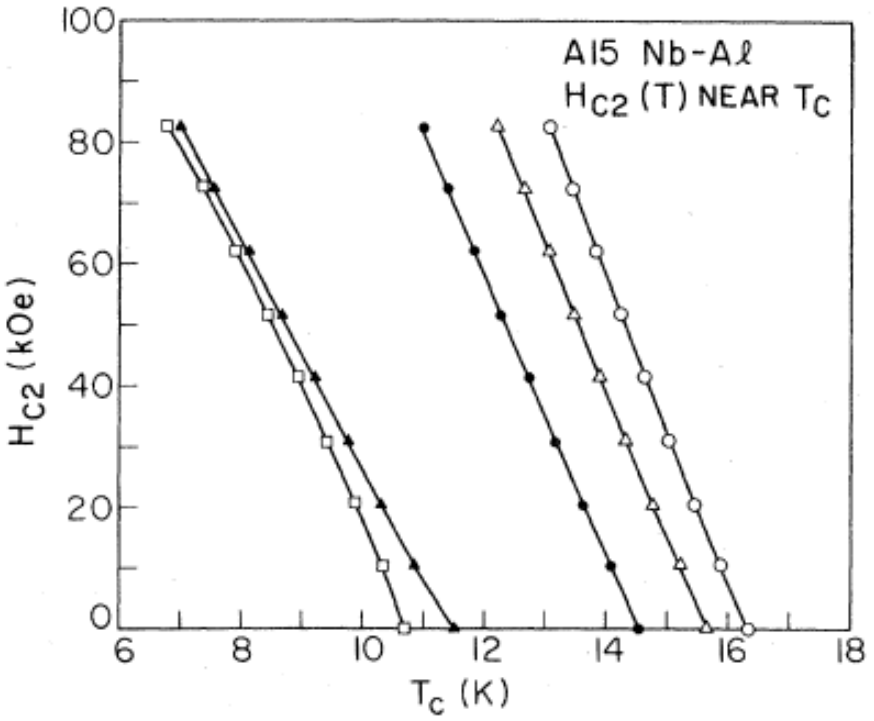

FIG. 1. Representative critical-field data near T_c of a series of *A*15 Nb-Al films measured. The lines drawn through data points are intended to serve only as a guide to the eye.

Based on the data of the critical-field slope near T_c, the general procedure of evaluating various superconducting and normal-state parameters including $N^b(0)$ is well formulated. Briefly, **the slope of critical field near T_c** including corrections for the electron-phonon interaction can be expressed as

$$\left.\frac{dH_{c2}}{dT}\right|_{T_c} = \eta_{H_{c2}}(T_c)\left[9.55\times10^{24}\gamma^{*2}T_c\left(\frac{n^{3/2}S}{S_F}\right)^{-2} + 5.26\times10^{4}\gamma^{*}\rho(\Omega\,\mathrm{cm})\right]\times[R(\gamma_{tr})]^{-1}\ \mathrm{Oe/K}\ ,$$

The electron-phonon spectral function $\alpha^2 F(\omega)$

Nb_3Sn

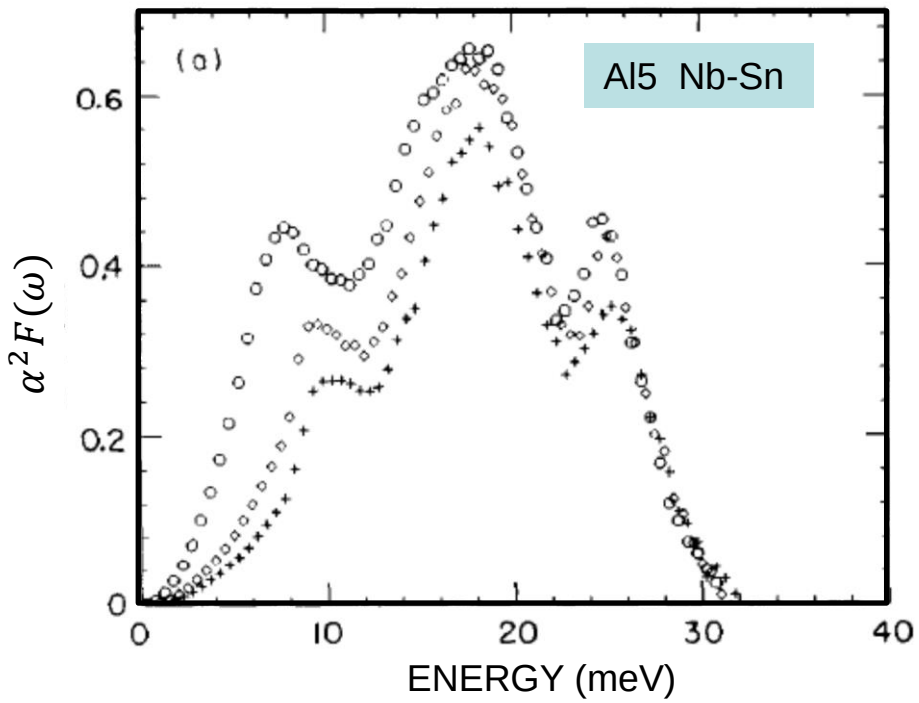

Nb_3Ge

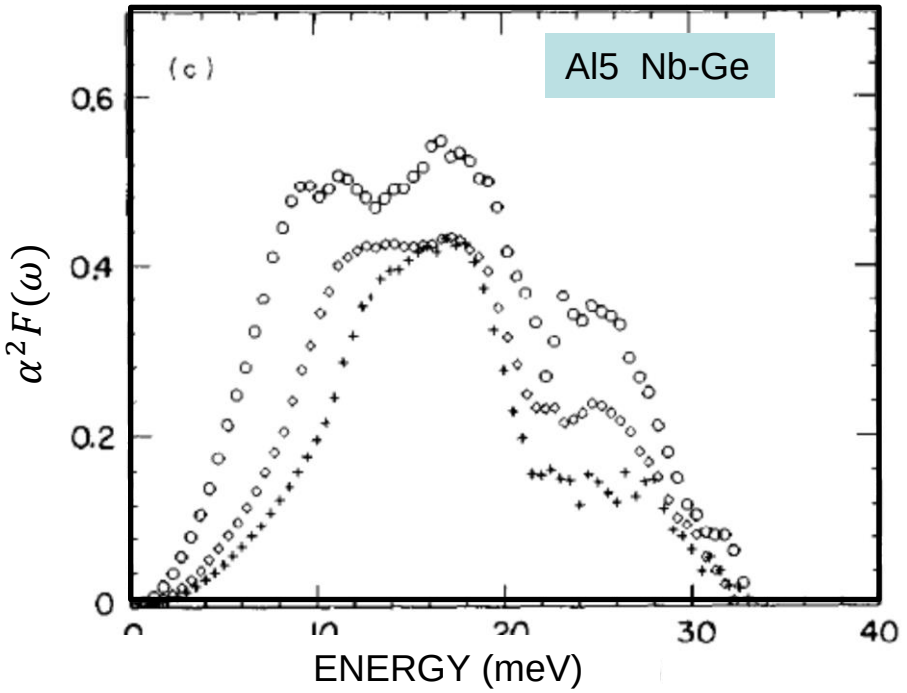

Nb tunnel junctions for Josephson device applications

Nb/Al/oxide/Pb junctions

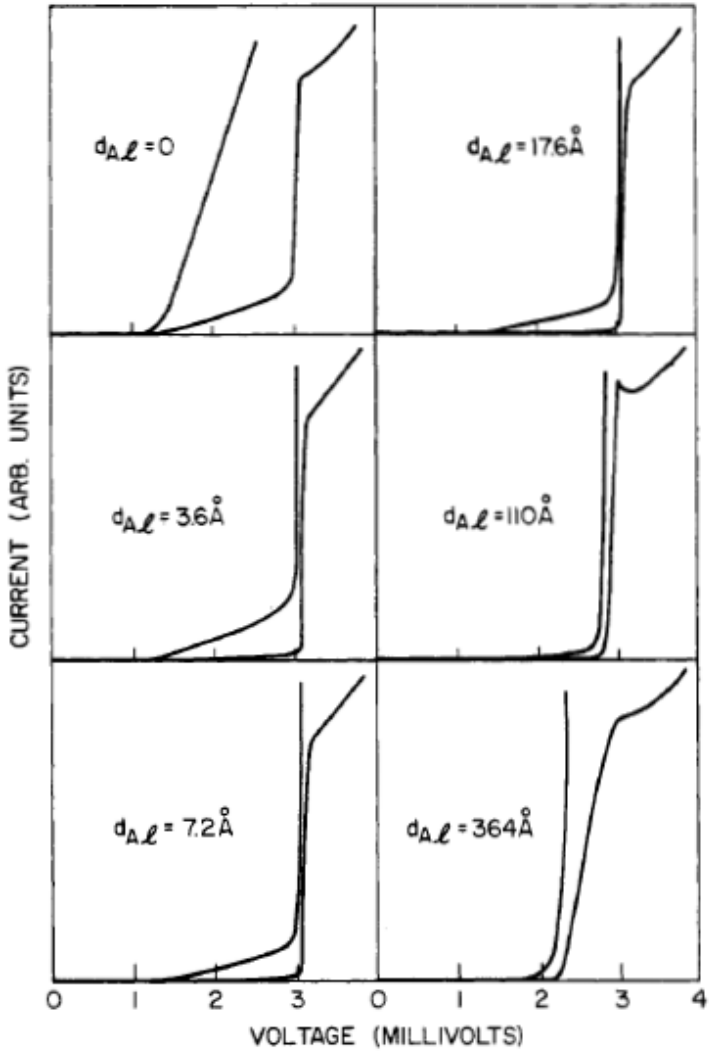

Fig. 2 Volt-ampere characteristics of Nb/Al-oxide-$Pb_{0.90}Bi_{0.10}$ junctions with different d_{Al} at $T \simeq 2^{o}K$. Expansion of the current scale ×10 is also shown. The junction without an Al overlayer was oxidized for 4 days, the rest for 20 min. All junctions have area $S \simeq 2 \cdot 10^{-3}$ cm^2.

Nb JOSEPHSON TUNNEL JUNCTIONS WITH THIN LAYERS OF Al NEAR THE BARRIER

M. Gurvitch, J. M. Rowell, H. A. Huggins,
M. A. Washington and T. A. Fulton

Bell Laboratories
Murray Hill, New Jersey 07974

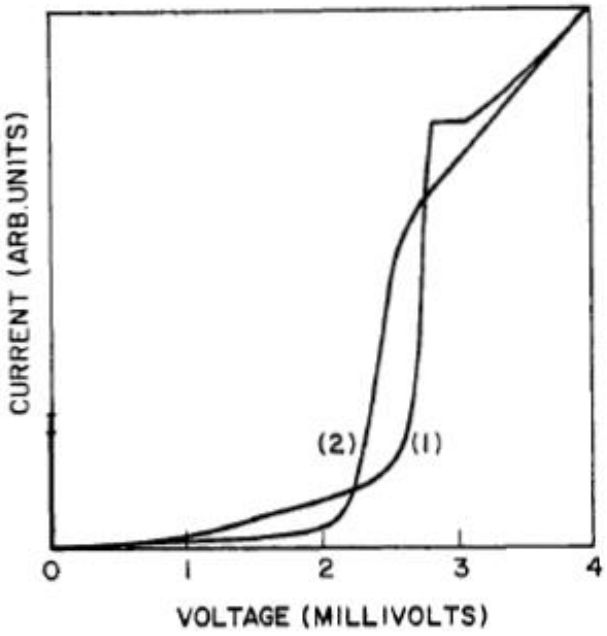

Fig. 3 Volt-ampere characteristics of Nb/Al-oxide-Nb (curve 1) and Nb/Al-oxide-Al/Nb (curve 2) junctions at $T \simeq 2^{o}K$. Both base electrodes have d_{Al} = 25Å, the top electrode of the junction with the second Al layer has d_{Al} = 32Å. Critical currents are ~50A/cm^2.

IEEE TRANSACTIONS ON MAGNETICS, VOL. MAG-19, NO. 3, MAY 1983

XPS and Tunneling Study of Air-oxidized Overlayer Structures of Nb with Thin Mg, Y and Er

J. Kwo
G. K. Wertheim
M. Gurvitch
D. N. E. Buchanan

Bell Laboratories
Murray Hill, New Jersey 07974

Artificial tunnel barrier made of oxides of thin Si, Mg, Y, and Er

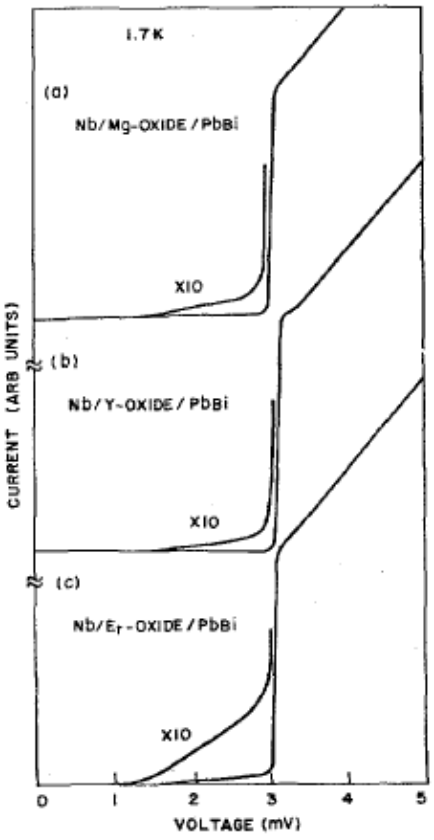

Fig. 2 Current-voltage characteristic of junctions of
(a) Nb/16.6Å Mg-oxide/$Pb_{0.9}Bi_{0.1}$, R = 21.7 Ω
(b) Nb/Y 8.7Å Y-oxide/$Pb_{0.9}Bi_{0.1}$, R = 181 Ω
(c) Nb/Er 4.5Å Er-oxide/$Pb_{0.9}Bi_{0.1}$, R = 20 Ω
The junction area is typically of $1.3 \times 10^{-2} cm^2$.

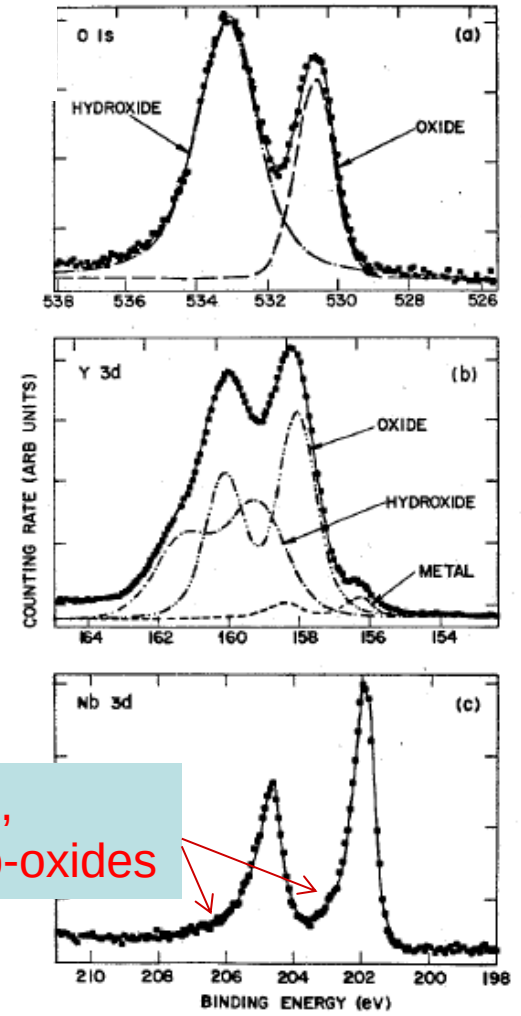

Very clean,
free of sub-oxides

Fig. 3 XPS data for a sample of Nb/30Å Y overlayer
(a) O 1s
(b) Y 3d
(c) Nb 3d

References

PHYSICAL REVIEW B VOLUME 23, NUMBER 7 1 APRIL 1981

Superconducting tunneling into the *A*15 Nb_3Al thin films

J. Kwo and T. H. Geballe*

Department of Applied Physics, Stanford University, Stanford, California 94305

PHYSICAL REVIEW B VOLUME 24, NUMBER 5 1 SEPTEMBER 1981

Microscopic superconducting parameters of Nb_3Al: Importance of the band density of states

J. Kwo,* T. P. Orlando,† and M. R. Beasley‡

Department of Applied Physics, Stanford University, Stanford, California 94305

(Received 12 December 1980)

PHYSICAL REVIEW B VOLUME 24, NUMBER 4 15 AUGUST 1981

Modification of tunneling barriers on Nb by a few monolayers of Al

J. M. Rowell, M. Gurvitch, and J. Geerk*

Bell Laboratories, Murray Hill, New Jersey 07974

(Received 10 June 1981)

VOLUME 63, NUMBER 9 PHYSICAL REVIEW LETTERS 28 AUGUST 1989

Reproducible Tunneling Data on Chemically Etched Single Crystals of $YBa_2Cu_3O_7$

M. Gurvitch, J. M. Valles, Jr., A. M. Cucolo,[(a)] R. C. Dynes, J. P. Garno, L. F. Schneemeyer, and J. V. Waszczak

AT&T Bell Laboratories, Murray Hill, New Jersey 07974

(Received 26 May 1989)

Observations of quasi-particle tunneling and Josephson behavior in $Y_1Ba_2Cu_3O_{7-x}$/native barrier/Pb thin-film junctions
J. Kwo, T. A. Fulton et al, Appl. Phys. Lett. **56**, 788 (1990).

5.2 Photon-assisted tunnelling

Book of Solymar

The tunnelling current may be modified by illuminating the junction with electromagnetic waves. It is easy to see that if the energy of the incident photons is in excess of 2Δ they will break up Cooper-pairs and create two electrons above the gap as shown in Fig. 5.5 (*a*). Since the number of electrons above the gap increases this way above its equilibrium value, some of these extra electrons will tunnel across the barrier (Fig. 5.5 (*b*)) creating thereby an extra current. We shall return to this problem in Section 7.2, for the moment we shall concentrate on the case when the energy of the incident photon is insufficient to break up a Cooper-pair. Influence on the tunnelling characteristics is still possible then if the photons act jointly with the applied voltage.

T = 0K

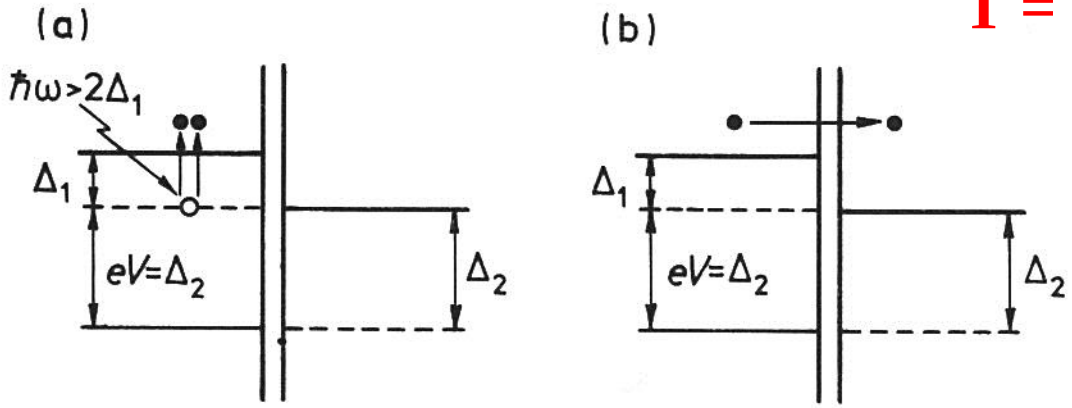

Fig. 5.5 Effect of incident photons on a tunnel junction; (*a*) a photon creates two electrons by breaking up a Cooper-pair, (*b*) one of the electrons created tunnels across.

Let us take $T = 0°\text{K}$ again and recall the case when $V = (\Delta_1 + \Delta_2)/e$. Then a Cooper-pair may break up into two electrons, one of them tunnelling across the barrier as has been shown in Fig. 4.12. If $V < (\Delta_1 + \Delta_2)/e$ no current flows. A Cooper-pair breaking up could not cause a current because the transition shown in Fig. 5.6 (*a*) with dotted lines is not permissible. However, if a photon of the right energy is available the liberated electron may follow the path shown in Fig. 5.6 (*b*) and get into an allowed state just above the gap. We may say that the electron tunnelled across the barrier by absorbing a photon, and refer to the phenomenon as photon-assisted tunnelling. The mathematical condition for the onset of tunnelling current is

for $eV < \Delta_1 + \Delta_2$

$$\hbar\omega = \Delta_1 + \Delta_2 - eV. \qquad (5.1)$$

T = 0K

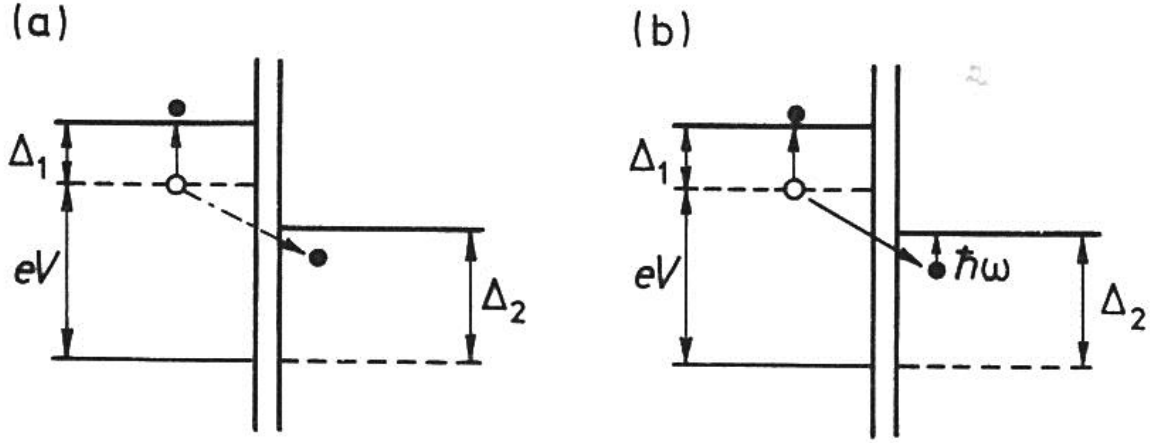

Fig. 5.6 (*a*) Tunnelling not allowed. (*b*) Tunnelling allowed if assisted by a photon.

If the energy of the photon is above this value tunnelling is still possible, though with a reduced probability because of a less favourable density of states. If the energy of the incident photon is below the value given by Equation (5.1) tunnelling may still be possible with the aid of a multi-photon process. An electron absorbing for example three photons simultaneously may tunnel across the barrier in the way shown in Fig. 5.7 (*a*). Hence we may expect sudden rises in the tunnelling characteristics whenever the condition

$$n\hbar\omega = \Delta_1 + \Delta_2 - eV \tag{5.2}$$

is satisfied, that is for a series of voltages in the range $0 < V < (\Delta_1 + \Delta_2)/e$.

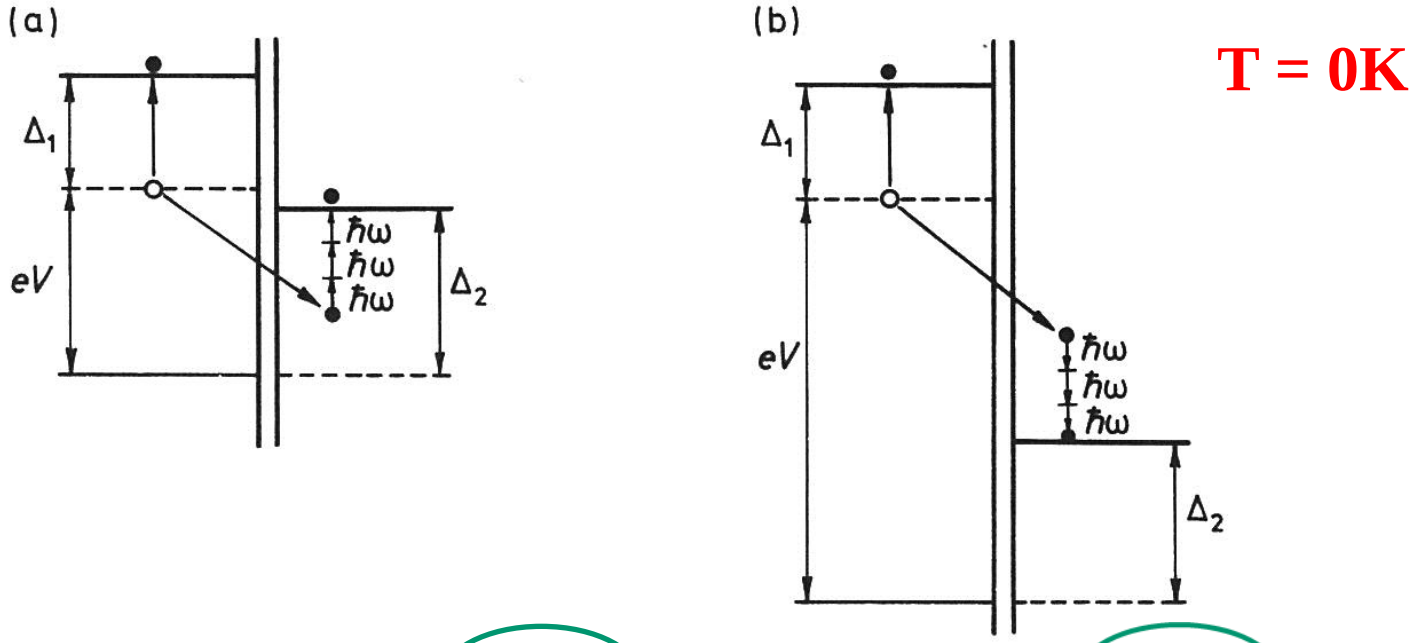

Fig. 5.7 Tunnelling assisted (*a*) by absorption of three photons, (*b*) by emission of three photons.

For $eV > \Delta_1 + \Delta_2$

When $V > (\Delta_1 + \Delta_2)/e$ we know that a tunnelling current will flow even in the absence of an incident electromagnetic wave. However, if photons of the right energy are available they can assist the tunnelling in this case as well, as shown in Fig. 5.7 (*b*) for a three-photon process. A Cooper-pair breaks up; one of the electrons goes into a state just above the gap on the left, and the other electron tunnels across into the superconductor on the right at an energy demanded by energy conservation (the sum of electron energies must equal the energy of the Cooper-pair). This process would occur with much higher probability if the electron could tunnel into the high density states lying just above the gap on the right. In Fig. 5.7 (*b*) this becomes energetically possible when three photons are *emitted* at the same time. Thus the mechanism of current rise is photon emission *stimulated* by input photons. For an *n*-photon emission process the current rises occur when

T = 0K

$$V_n = \frac{1}{e}(\Delta_1 + \Delta_2 + n\hbar\omega). \tag{5.3}$$

T > 0K

For finite temperatures there is one more instance where electrons tunnel between maximum density states and that occurs at $V = (\Delta_2 - \Delta_1)/e$, as shown in Fig. 5.8 (*a*). Tunnelling between those states may also be assisted by photons as shown in Figs. 5.8 (*b* and *c*) for photon absorption and emission respectively. In general, multi-photon absorptions and emissions are possible again, and thus for finite temperatures there is another set of voltages,

$$V_m = \frac{1}{e}(\Delta_2 - \Delta_1 + m\hbar\omega), \qquad m = \pm 1, \pm 2, \pm 3 \tag{5.4}$$

at which current rises can be expected.

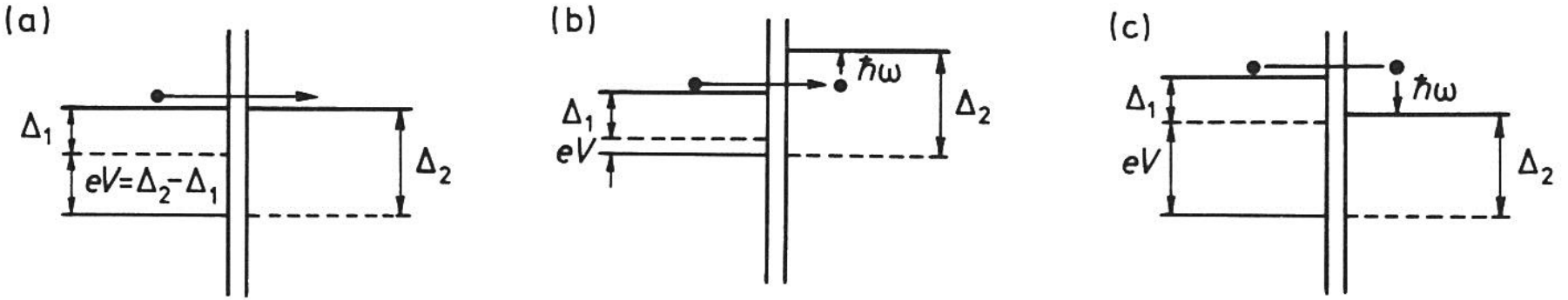

Fig. 5.8 Tunnelling between maximum density states at finite temperature (*a*) directly, (*b*) by photon absorption, (*c*) by photon emission.

The first experiments on tunnel junctions in the presence of electromagnetic waves were performed by Dayem and Martin [57] using junctions between Al and Pb, In or Sn. The frequency of the electromagnetic wave employed was 38·83 GHz so the experimental solution was to place the sample inside a cavity. The current–voltage characteristic was measured and rises in current were indeed found as may be seen in Fig. 5.9 (*a*) where the solid and dotted lines show the characteristic in the absence and presence of microwaves respectively.

Quantitative explanations were given nearly simultaneously by Tien and Gordon [58] and Cohen, Falicov and Phillips [126]. The methods in their papers were different but obtained essentially the same results. Cohen, Falicov and Phillips assumed that the magnetic field of the microwaves modulates the energy gap, whereas Tien and Gordon added an electrostatic perturbation term to the Hamiltonian. We shall follow here the latter derivation.

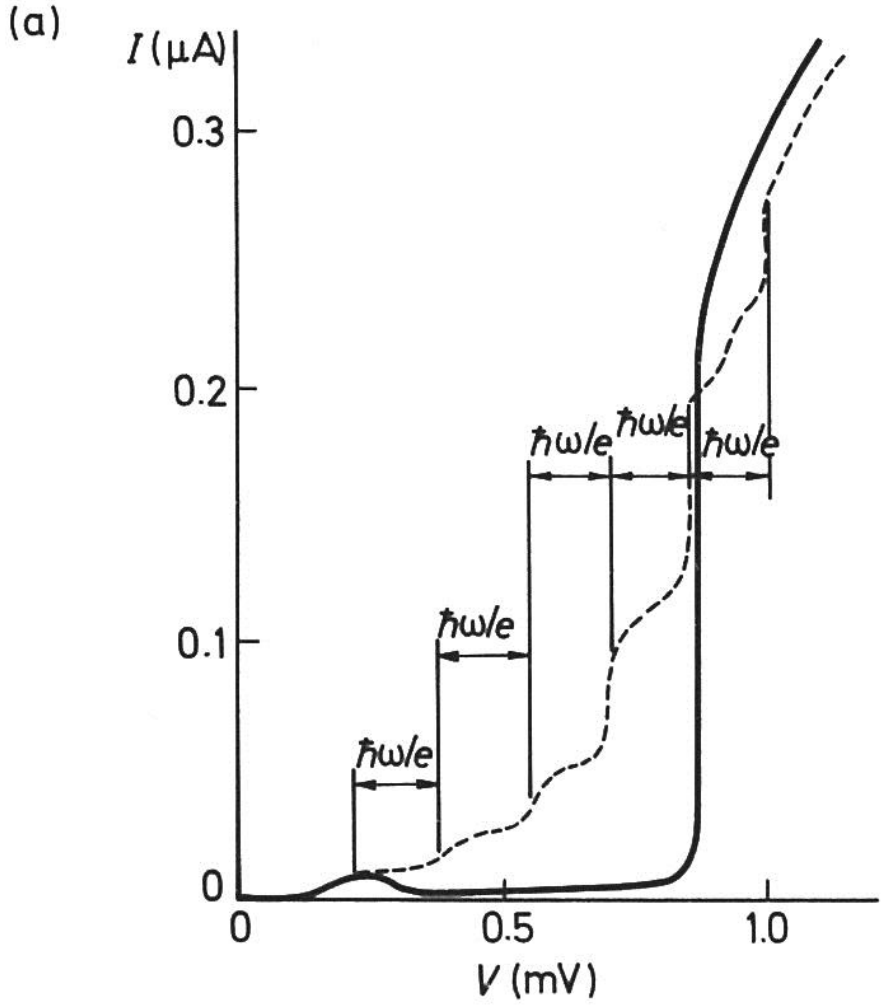

Fig. 5.9 (*a*) *I–V* characteristic of an Al–I–In junction in the absence (solid lines) and presence (dotted lines) of microwaves of frequency 38·83 GHz. Measurements by Dayem and Martin, quoted by Tien and Gordon [58].

The simplest assumption one can make is to regard the junction as a capacitance with a time-varying but spatially constant electric field between the plates. Regarding the potential of one of the superconductors (2) as the reference we may argue that the only effect of the microwave field is to add an electrostatic potential of the form

$$V_{\mathrm{rf}} \cos \omega t \tag{5.5}$$

to the energy of the electrons in the other superconductor (1). Hence, for electrons in superconductor (1) we may use the new Hamiltonian

$$H = H_0 + eV_{\mathrm{rf}} \cos \omega t \tag{5.6}$$

where the first term is the unperturbed Hamiltonian in the absence of microwaves.

If the unperturbed wavefunction was

$$\Psi_0(x, y, z, t) = f(x, y, z) \exp(-iEt/\hbar) \tag{5.7}$$

then the solution for the new wavefunction may be sought in the form

$$\Psi(x, y, z, t) = \Psi_0(x, y, z, t) \sum_{n=-\infty}^{\infty} B_n \exp(-in\omega t). \tag{5.8}$$

Substituting Equation (5.8) into Schrödinger's equation

$$H\Psi = i\hbar\frac{\partial\Psi}{\partial t} \tag{5.9}$$

we find

$$2nB_n = \frac{eV_{\mathrm{rf}}}{\hbar\omega}(B_{n+1} + B_{n-1}) \tag{5.10}$$

which is satisfied by [101]

$$B_n = J_n(eV_{\mathrm{rf}}/\hbar\omega) \tag{5.11}$$

where J_n is the n_{th} order Bessel function of the first kind. The new wavefunction is then

$$\Psi(x, y, z, t) = f(x, y, z, t)\exp(-iE\hbar/t)\sum_{n=-\infty}^{\infty} J_n(\alpha)\exp(-in\omega t), \tag{5.12}$$

where

$$\alpha = \frac{eV_{\mathrm{rf}}}{\hbar\omega}. \tag{5.13}$$

It may be seen that in the presence of microwaves the wavefunction contains components with energies

$$E, E \pm \hbar\omega, E \pm 2\hbar\omega, \ldots \tag{5.14}$$

respectively. Without the electric field, an electron of energy E in superconductor (1) can only tunnel to the states in superconductor (2) of the same energy. In the presence of the electric field, the electron may tunnel to the states in superconductor (2) of energies E, $E \pm \hbar\omega$, $E \pm 2\hbar\omega$, etc. Let $N_{20}(E)$ be the unperturbed density of states of the superconductor (2). In the presence of microwaves we then have an effective density of states given by

$$N_2(E) = \sum_{n=-\infty}^{\infty} N_{20}(E + n\hbar\omega) J_n^2(\alpha). \tag{5.15}$$

We may now obtain the tunnelling current by substituting Equation (5.15) into the general expression Equation (2.14), yielding*

$$I = A \sum_{n=-\infty}^{\infty} J_n^2(\alpha) \int_{-\infty}^{\infty} N_1(E-eV) N_{20}(E+n\hbar\omega)\left[f(E-eV)-f(E+n\hbar\omega)\right] dE$$

$$= A \sum_{n=-\infty}^{\infty} J_n^2(\alpha) I_0(eV+n\hbar\omega) \tag{5.16}$$

where $I_0(eV)$ is the tunnelling current in the absence of microwaves.

In the limit $\hbar\omega \to 0$ it may be shown (see Appendix 5) that the above expression reduces to the classical value

$$I = \frac{1}{\pi} \int_{-\pi/2}^{\pi/2} I_0(V + V_{\mathrm{rf}} \sin \omega t)\, d(\omega t). \tag{5.17}$$

The comparison between theory and experiments has a long and tangled story. The first attempt was made by Tien and Gordon [58] who could reproduce the experimental results of Dayem and Martin [57] by taking $\alpha = 2$ as shown in Fig. 5.9 (*b*). The experimental value of α (that is the voltage in the junction) was, however, not known. Estimates by Tien and Gordon indicated a discrepancy as large as an order of magnitude.

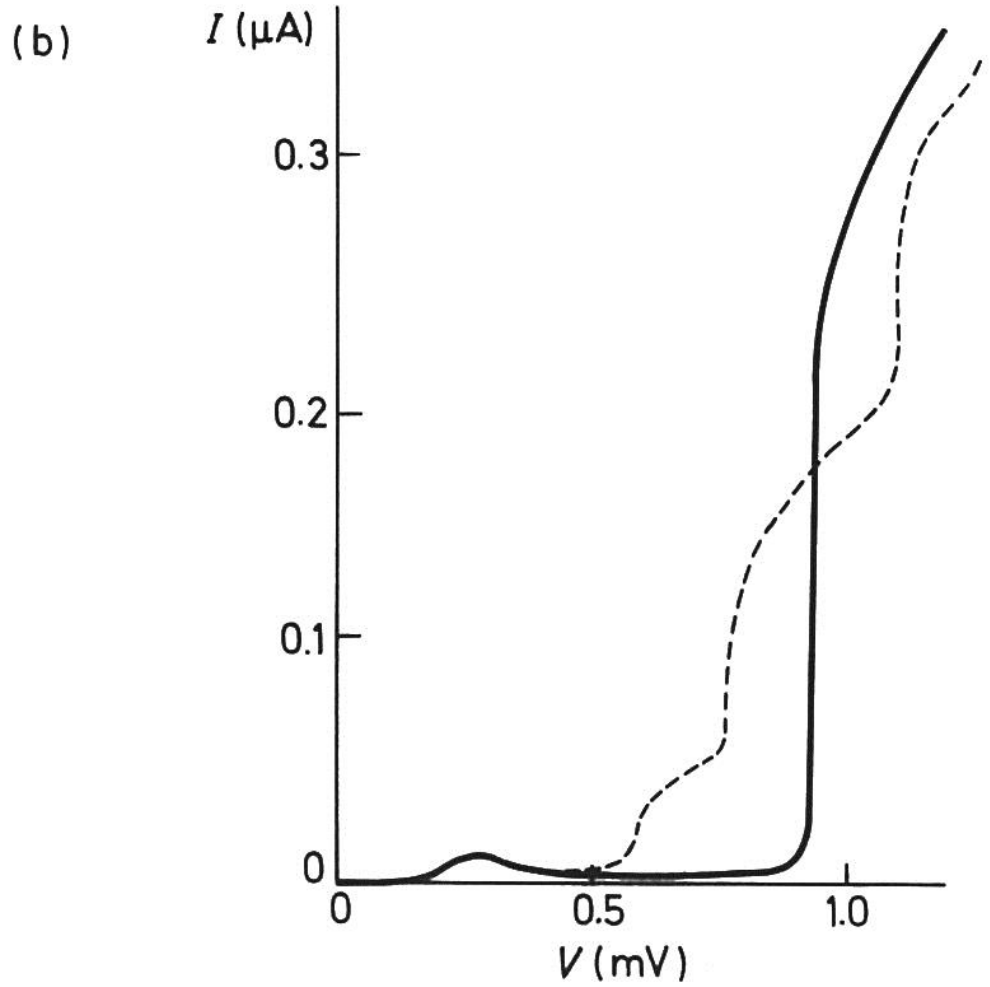

Fig. 5.9 (*b*) Theoretical curves by Tien and Gordon [58] for $\alpha = 2$.

To prove the point that it is the spatial variation which is responsible for the discrepancy, Hamilton and Shapiro [135] conducted another series of experiments on a very small (hardly overlapping in an in-line geometry) junction. The results then did agree with the Tien–Gordon theory as shown in Fig. 5.15.

Two more proofs in favour of the Tien–Gordon theory are the measurements of Hamilton and Shapiro [135] at 200 Hz where V_{rf} could be easily measured and the microwave experiments of Longacre and Shapiro [137] conducted on point contact (that is, very small) junctions.

Shapiro steps to the n^{th} order

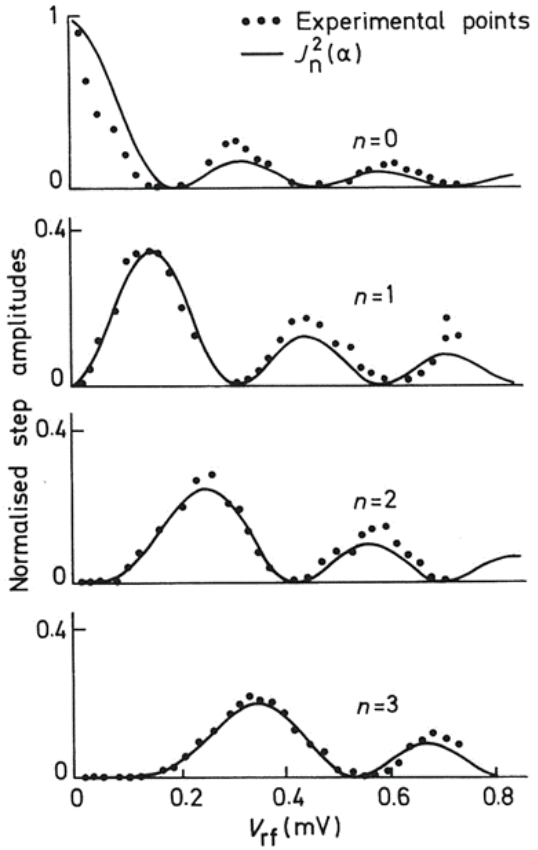

Fig. 5.15 Same as Fig. 5.14 for a very small junction. After Hamilton and Shapiro [135].